This is to certify that the

dissertation entitled

Methods for Absorbance-Corrected Chemiluminescence and Fluorescence

presented by

Eugene Ratzlaff

has been accepted towards fulfillment
of the requirements for

Doctoral degree in Chemistry

Major professor

Date 12/21/82

METHODS FOR ABSORBANCE-CORRECTED CHEMILUMINESCENCE AND FLUORESCENCE

By

Eugene Henry Ratzlaff

A DISSERTATION

Submitted to
Michigan State University
in partial fulfillment of the requirements
for the degree of

DOCTOR OF PHILOSOPHY

Department of Chemistry

1982

G120605

ABSTRACT

METHODS FOR ABSORBANCE-CORRECTED CHEMILUMINESCENCE AND FLUORESCENCE

By

Eugene Henry Ratzlaff

A mathematical model of the secondary inner-filter effect in chemiluminescent solutions has been developed to account for measurement errors due to the attenuation of radiation by absorption. This model has allowed the derivation of a correction function based on a determination of the ratio of chemiluminescence intensities from two pathlengths. Luminol chemiluminescence was observed from solutions containing the interfering chromophores picrate and ferroin. Absorption-free signals are accurately calculated for matrices with absorbances ranging to more than 0.75. An emission spectrum demonstrating ferroin catalysis is recovered from an apparently quenched reaction.

A flow cell has been designed for simultaneous fluorescence and absorbance measurements. A bifurcated fiber-optic is used for excitation and front-surface fluorescence collection. Convolution of mathematical descriptions for primary and secondary absorbance effects and the fiber-optic/cell light transfer function results in a model for an inner-filter effect correction function. The absorbance-corrected emission of quinine sulfate is a linear function

of concentration from 0.1 μM to 400 μM, despite self-absorption values extending to 3.0. Fluorescence signals are corrected for primary and/or secondary absorbances in excess of 3.0.

Microcomputer-interfaced instrumentation and software were developed for these luminescence experiments. A versatile, programmable timer/counter and a simultaneous sampling, quad input analog-to-digital data acquisition interface were used. A low cost photodiode detector was engineered for stability and wide dynamic range. A hierarchical computing environment provided the software power and hardware flexibility needed to implement these systems.

A mathematical luminescence volume-source model was developed for evaluation and development of these absorption-correction methods. The model verifies a collimation assumption required for the absorbance-corrected chemiluminescence method. Derivation of equations for the absorbance-corrected fluorescence technique required an understanding of the fiber-optic/cell transfer function which was evaluated with the luminescence volume-source model.

To Jewel,

to my parents,

and to my family

ACKNOWLEDGMENTS

My gratitude and thanks go to Professor Stanley Crouch for his support, friendship, and for many freedoms enjoyed under his guidance. I am indebted to Professor Chris Enke for his contribution as second reader, and to the other members of my committees, Professors Clarence Suelter, Jack Holland, and James Dye.

Many others should be held responsible. Foremost among these is Charlie Patton, whose companionship helped make my work creative and my frustrations bearable. I shall not soon forget many, many others from whom I learned and benefited, and with whom I shared friendships - Dave Christmann, Jim Gano, Clay Calkin, Rytis Balciunas, Rob Thompson, Frank Curran, Pete Aiello, Paul Kraus, Keith Trischan, Pat Wiegand, John Stanley, Marguerite Martin, Siriwan 'Kim' Ratanathanawongs, Mark Victor, and Bob Harfman, to name just a few. Many members of the Enke group are particularly culpable, others of you are certainly aware of your complicity.

I gratefully acknowledge many others for their invaluable expert help, advice, and craftsmanship: Professor Andrew Timnick, Dr. Tom Atkinson, Marty Rabb, Russ Geyer, Dick Menke, Ron Haas, Scott Sanderson, John Funkhouser, Andy Seer, Jo Kotarski, and other staff and friends.

TABLE OF CONTENTS

TABLE OF CONTENTS

Chapter Page

Chapter Page

LIST OF TABLES

LIST OF FIGURES

Figure | Page

CHAPTER 1

INTRODUCTION

Molecular luminescence methods have gained a great deal of popularity within the scientific community due to their versatility and broad applicability. Luminescence methods are useful because of their high sensitivity and excellent selectivity. Luminescence is often more selective than absorption because two wavelength selectors, emission and excitation are used. In addition, luminescence polarization and luminescence lifetimes can be used to enhance selectivity. However, there are large numbers of instrumental difficulties as well as physical and chemical interferences, and these problems can prevent many potential applications from being realized. One such problem is the attenuation of luminescence signals due to the absorption of light by the analyte itself, or by other components in the matrix, often known as the inner-filter effect.

Methods of describing and correcting for inner-filter effects are the major concern of this thesis. The ultimate objective of this field of research is the development of techniques and instrumentation with all of the capabilities, sensitivity, and ease of use of modern commercial automated instruments, but with the added feature of automated self-detection and correction of inner-filter effects. With this should come new analytical procedures made possible by this

improved methodology.

The problem of secondary absorption (absorption of the emitted radiation) in chemiluminescent solutions is discussed in the second chapter of this thesis. A mathematical model of secondary absorption effects is developed, and a correction factor is derived. The instrument and chemistry developed for implementation and testing of the model are evaluated.

The third chapter is concerned with some aspects of the primary absorption effect (absorption of the exciting radiation) with front surface fluorescence techniques. A difficult requirement in determining inner-filter effect correction factors is describing the fluorescing solution as a volume source, rather than as a point source. The volume source becomes more amenable to mathematical modeling if the observed light can be collimated. Unfortunately, this creates a severe limitation in light throughput. The instrument developed in this work uses a bifurcated fiber-optic as an excitation-emission window with a transmittance flow cell. Absorbance and fluorescence are simultaneously available. This information is used with a correction model that mathematically describes this fiber-optic/cell configuration. Because the collimation requirement of earlier correction methods has been eliminated, the acceptance function of this configuration is improved over earlier instruments. Vastly improved sensitivities are predicted. The theory for development of the model and the results of testing and evaluation are presented.

Instrumentation and software are discussed in the fourth chapter. A description of the hierarchical computing system and microcomputer

used for these experiments is presented. A counting/timing module, a sample-and-hold/multiplexer module, and an analog-to-digital converter module were designed by the author. A photodiode detector system is also presented here. Two microcomputing languages, SLOPS and FORTH, are compared and illustrated as languages for these experiments.

A volume source model for luminescence methods is developed and discussed in Chapter V. This model permits assumptions in the absorbance-corrected chemiluminescence technique to be tested and proven. The model is also required for the development of the absorbance-corrected fluorimeter, as described in Chapter III. Modeling and fitting of the fluorescent solution as a volume rather than a point source is a key requirement of the efficiently coupled fiber-optic fluorescence cell.

The final chapter summarizes the current work and projects to future work. Many improvements at both theoretical and instrumental levels are possible. Hopefully, absorbance-corrected luminescence techniques will one day be readily available tools for routine application in many areas of chemical analysis.

CHAPTER II

ABSORBANCE-CORRECTED CHEMILUMINESCENCE MEASUREMENTS WITH A DUAL-PATHLENGTH SPECTROMETER

A. Introduction and Historical

1. Principles of Chemiluminescence

Chemiluminescence (CL) is the emission of light resulting from a chemical reaction. In general, chemiluminescence is a result of the promotion of a molecule into the excited state during a chemical reaction followed by subsequent decay to the ground state accompanied by light emission. Chemiluminescence is most commonly observed in biological systems such as fireflies and luminescent bacteria and algae found in the sea. This special form of chemiluminescence is appropriately called bioluminescence and is frequently an enzyme-catalyzed process.

Early studies of bioluminescence have led to greater interest in chemiluminescence in general among biologists, biochemists, and chemists. Bioluminescence was first used analytically in 1889 by Beijerink (1) for the detection of low-level oxygen with luminescent bacteria. Since that time a few chemiluminescence assays have become established as sensitive and selective methods for the determination of trace metals, hydrogen peroxide, ATP, and NADH. Analytical chemiluminescence methods are useful because they provide excellent sensitivity, adequate selectivity, and linear response. The inherent

sensitivity of luminescence is complemented by the added simplicity and advantage of not requiring a source for optical excitation. The added sensitivity of enzyme multiplication is also possible with many bioluminescence methods. Bioluminescence also has the advantage of the specificity associated with many enzyme-catalyzed reactions. Most commonly used chemiluminescence reactions have half-lives of less than 10 seconds, and this allows rapid analysis times and high throughput. Wide linear response has been demonstrated for a variety of chemiluminescence methods. Low reagent and sample consumption is also a result of the high detection sensitivity. Complete reviews of chemiluminescence are available in the literature (2-7).

2. Problems with Chemiluminescence Methods

Among hindrances to further analytical applications of chemiluminescence techniques is the non-specificity of many chemiluminescent reactions. For this reason, many methods require a prior separation of analytes before chemiluminescence detection. Another problem is the interference attributable to inner-filter effects (attenuation of emitted light intensity due to absorbance by the solution matrix). When chemiluminescence is detected, any absorbance of chemiluminescent radiation within the solution, or any variation in absorbed chemiluminescence from solution to solution results in a difference between the amount of light actually detected, and the amount of light anticipated or expected. If the amount of light detected is to be correlated with the concentration of an analyte or the spectral distribution and radiant power of emission,

these values will be in error. Several such problems with inner-filter effects have been described.

Wampler, et. al. (8) demonstrated a problem with the inner-filter effect of riboflavin in a luciferin-luciferase reaction coupled to peroxide-forming reactions of clinical and biochemical interest. Van Dyke, et. al. (9) mention the importance of eliminating erythrocyte contamination to avoid inner-filter effects in a blood screening system using luminol chemiluminescence. In the chemiluminescent determination of humic acid by reaction with permanganate, Marino and Ingle (10) have described signal attenuation due to the appreciable absorbance of humic acid in the higher concentration range.

Inner-filter effect interferences with chemiluminescence spectroscopy are analogous to secondary absorption interferences in fluorescence spectroscopy (absorption of fluorescence emission). Methods of correction of secondary absorption in fluorescence spectroscopy have been reviewed elsewhere (11-13). These descriptions of fluorescence secondary-absorption corrections are complicated by and dependent on the primary absorbance of excitation radiation and the convolution of excitation and emission geometries. Most are concerned with the multiple reabsorption and reemission effects of a single fluorophore. Experimental evidence, thoroughness, and clarity are often lacking; these methods have not been found to be directly useful for chemiluminescence inner-filter effect correction.

Although no remedy for inner-filter effect interferences with chemiluminescence methods has been reported, an expression describing chemiluminescence in terms of absorbance and pathlength was given by Stieg and Nieman and applied as a criterion for the efficient design

of chemiluminescence flow cells (14). Experimental results were superimposed on a theoretical chemiluminescence response curve for various pathlengths. The gallic acid chemiluminescent reaction system was observed at 643 nm at concentrations where the absorbance per unit pathlength was 1.6. Requirements and limitations of the model's geometry were not stressed, nor were the effects of reemission or deviations from monochromaticity discussed. The expression of Stieg and Nieman has not been applied for modeling a correction method for inner-filter effects.

The following pages describe a procedure for correcting chemiluminescence measurements that is based on a determination of the ratio of chemiluminescence from two different cell pathlengths. A microprocessor-controlled instrument with a unique dual-path cell is described. The instrument automatically produces absorption-corrected chemiluminescence intensities at a single wavelength or absorption-corrected chemiluminescence spectra. Results of studies with a luminol chemiluminescent reaction are presented that demonstrate the effectiveness of the correction procedures and the characteristics of the instrument.

The basic premise behind this method of absorption-corrected chemiluminescence as well as that of corrected fluorescence by the method of cell shift and other methods, is that the emission attenuation is a well behaved (Beer's law) function of pathlength, and that the intensity vs. pathlength information is useful for identifying the corrected intensity. Interestingly, this approach is quite analogous to the method of "Recognition by Sight" as discussed in the classic Flatland by Edwin A. Abbott (15). In Flatland, a two

dimensional world lying in a single plane, all persons have the form of an equilateral polygon and class distinction is determined by the number of sides. A Flatlander (having been educated in the Science and Art of Sight Recognition) is able to distinguish the shape and thus, most importantly, the rank of another approaching Flatlander only because of the presence of Fog. Without Fog, all polygons appear as lines (recall that the observer is in the same plane). However, in the presence of Fog a line grows dimmer as it recedes, and by careful observation of the comparative dimness or clearness along the line the Flatlander can infer the acuteness of angles and thus the numbers of sides of an approaching person. The reader may find this reference useful for an intuitive insight into absorbance-corrected luminescence techniques.

A. Theory

1. Attenuation by Inner-Filter Effect

Consider a thin slice of solution of infinitesimal thickness dx, parallel to the observation window. The slice radiates monochromatic light of unattenuated radiant power dP_0, normal to the plane of the window, as shown in Figure 1-1. If an absorber is present between the slice and the window, the radiant power observed at the window, dP_x, is described by Beer's law as

$$dP_x = dP_0(10^{-\varepsilon cx}) = dP_0(e^{-2.303\varepsilon cx}) \qquad (2\text{-}1)$$

where ε is the molar absorptivity of the absorber, c is its

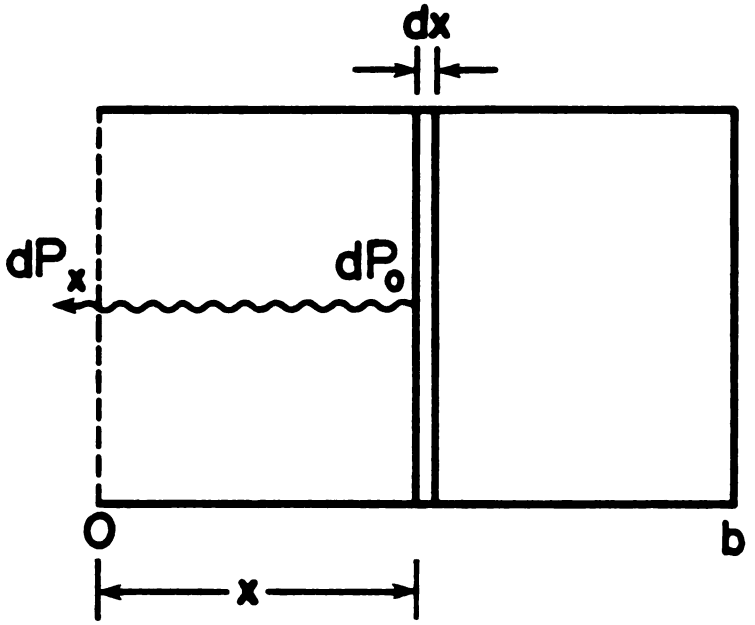

Figure 2-1. Schematic cell model.

concentration, and x is the distance of the slice from the cell window. The equation

$$dP_0/dx = J_0 d\Omega dA \qquad (2\text{-}2)$$

describes the unattenuated power per unit thickness as the product of the unattenuated radiant emissivity J_0, the solid angle of observation $d\Omega$, and the projected area dA of the radiating slice. By combining Equations 2-1 and 2-2, the observed radiant power can be expressed as a function of the slice thickness dx:

$$dP_x = (J_0 d\Omega dA)(e^{-2.303 \varepsilon c x})dx \qquad (2\text{-}3)$$

The total power observed P_b, for all slices within a cell of pathlength b is determined by integrating Equation 2-3 over all thicknesses from zero to b:

$$P_b = (J_0 d\Omega dA)\int_0^b (e^{-2.303 \varepsilon c x})dx \qquad (2\text{-}4)$$

Equation 2-4 reduces to

$$P_b = (J_0 d\Omega dA)(1-e^{-2.303 \varepsilon b c})/(2.303 \varepsilon c) \qquad (2\text{-}5)$$

(This is similar to Equation 10 of Stieg and Nieman (14) where r = 0). Note that in the limit of small εc, the observed radiant power is equal to the "absorption-free" radiant power P_0, and Equation 2-4 becomes

$$\lim_{\varepsilon c \to 0} P_b = P_0 = (J_0 d\Omega dA)b \qquad (2\text{-}6)$$

Since many chemiluminescent reactions result in chemically excited fluorescence of product molecules, the additional requirement that

light absorbed must not be reemitted (no overlap of excitation and emission spectra) must be included. Scattered light, refractive index effects, and reflections within the cell are assumed to be negligible.

2. The Dual-Path Method of Correction

Herein is proposed a method of chemiluminescence detection that simultaneously and conveniently determines the value of εc (and thus the absorbance $A = \varepsilon bc$) and the corrected radiant power P_0. The method is based on the comparison of luminescence measurements simultaneously taken from either length of a cell having pathlengths b' and b, where $b' < b$. The ratio R of these intensities can be found from Equation 2-5, yielding

$$R = P_{b'}/P_b = (1-e^{-2.303\varepsilon b'c})/(1-e^{-2.303\varepsilon bc}) \qquad (2-7)$$

With the known pathlength values b' and b, and the measured values of $P_{b'}$ and P_b, the value of εc can be determined from Equation 2-7 with an iterative approach. The corrected radiant power P_0 is then determined by substituting εc and the experimentally observed P_0 into Equation 2-8, which follows from Equations 2-5 and 2-6:

$$P_0 = 2.303P_b\varepsilon bc/(1-e^{-2.303\varepsilon bc}) \qquad (2-8)$$

C. Experimental

1. Apparatus

To investigate this model, a cell and collimator were designed to allow the measurement of the ratios of chemiluminescence from an homogeneous solution at 2 pathlengths as shown in Figure 2-2. The cell was made with the arbitrarily chosen nominal pathlengths of 1.00 and 0.50 cm. Black Delrin (16) was chosen as the construction material for both the cell and collimator because of its chemical inertness, machinability, and relatively low reflectivity. The cell was formed by machining the desired openings from a solid Delrin block, 45 mm wide at the front, 25 mm high, and 30 mm deep. The front opening was 15 mm high by 26 mm wide by 5 mm and 10 mm deep for the short and long pathlengths,respectively, cut 3 mm from the bottom of the block, as shown to scale in Figure 2-2, in a cut-away view from the top. A quartz microscope slide, 17 mm high by 30 mm wide, was cut to shape, press-fit into place, and sealed with black silicone rubber sealant (17) to form the cell window. An 8 mm diameter hole and a 3 mm diameter hole were drilled above the long and short sides of the cell, respectively, to allow solutions to be placed into or removed from the cell. The collimator was made by drilling a 2 mm diameter hole into a 50 mm long black Delrin rod. This diameter-to-length ratio yields an acceptance angle of approximately 2°, which gives a reasonable degree of collimation as required by the model, at the expense of some loss in radiant energy throughput.

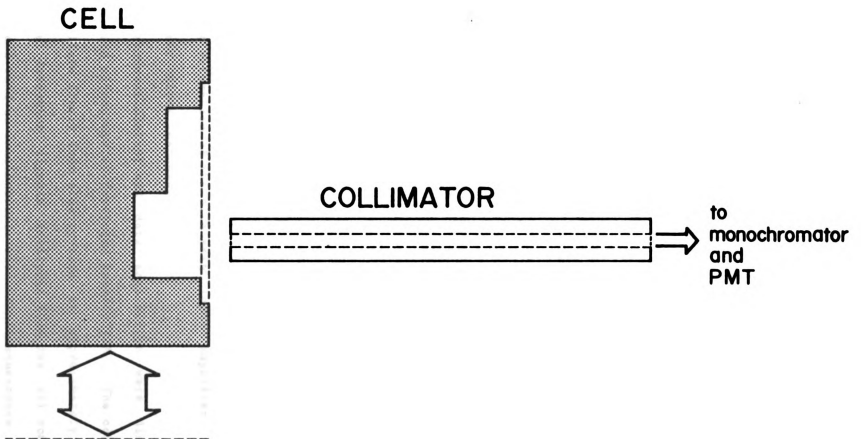

Figure 2-2. Top view diagram of dual-path CL cell and collimator.

The cell and collimator were mounted in a programmable sample chamber (18) with the collimator 5 mm from the cell window and centered in the exit port. The sample chamber was integrated into the optical system as shown in Figure 2-3. A 2 mm exit slit and the 2 mm diameter of the collimator at the entrance to the monochromator (19) resulted in a 16 nm spectral bandpass. All measurements were made at 425 nm unless otherwise noted. The Hamamatsu R928 photomultiplier tube (PMT) was cooled to reduce the dark current shot noise contrubution (12,20). Dark current was reduced more than 2 orders of magnitude from the room temperature value to a point where the dark current and dark current shot noise were lower than the amplifier noise and drift. Elimination of the dark current shot noise contribution resulted in enhancement of the signal-to-noise ratio by a factor of 5 to 10, depending upon the light level. The PMT voltage was -560 V; the output current was converted to voltage with a current amplifier (21) set at 10^{10} V/A gain and 10 ms rise time (10%-90%). Although output voltages were always well below 1 V, neither higher amplifier gain nor higher electron multiplier voltages were chosen. This allowed sufficient amplifier "headspace" for the fast-rising current input pulses. Higher amplification would have resulted in frequent saturation of the high gain input amplifier, resulting in non-linear output response.

Instrument control and data acquisition were directed by an 8085-based microcomputer developed locally (22). The cell was allowed to oscillate freely from side-to-side at approximately 2 Hz. Cell position detection signals available from the cell compartment were sensed and used to synchronously gate chemiluminescence measurements.

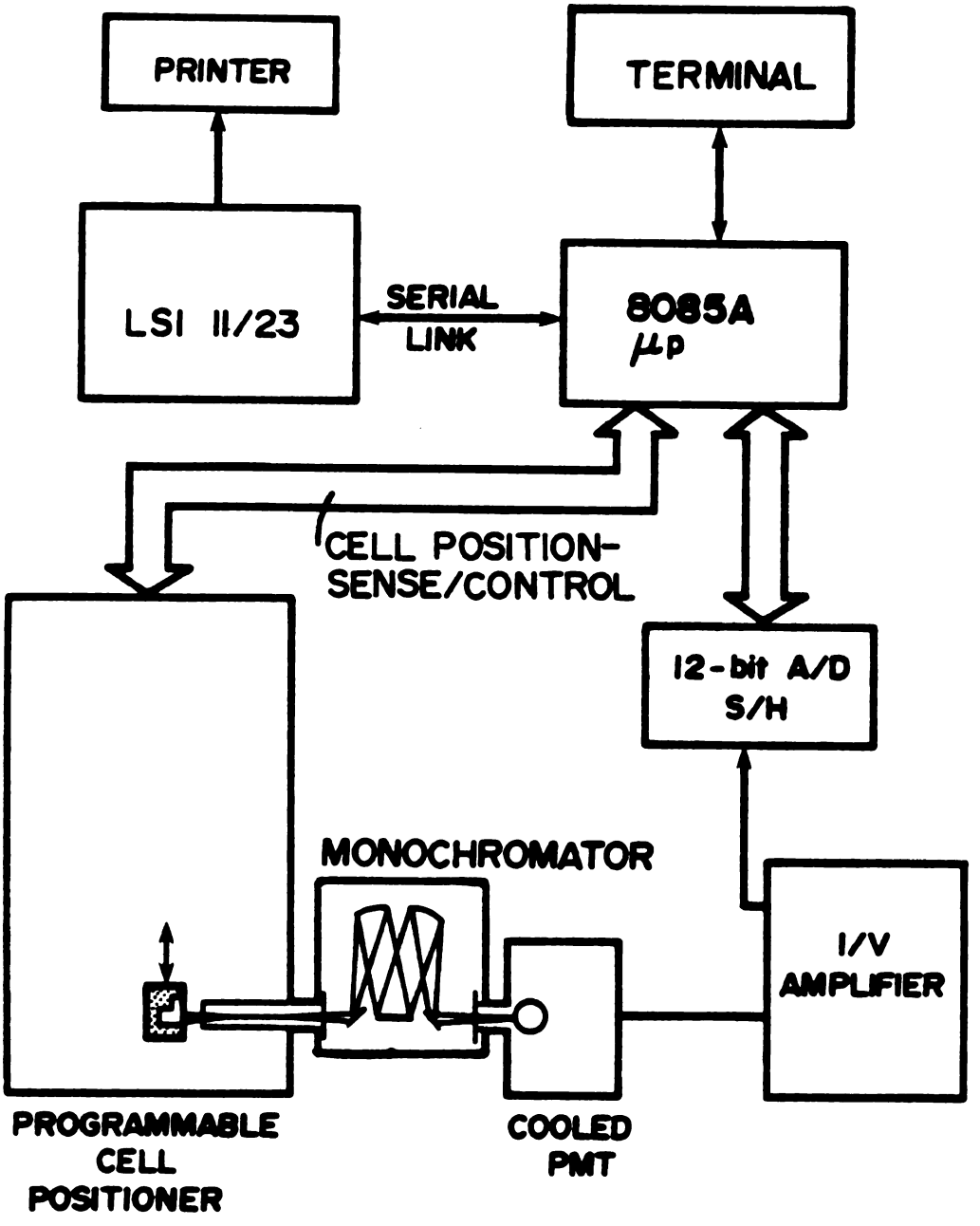

Figure 2-3. Schematic diagram of instrument.

At 2 samples per oscillation and 2 oscillations per second, the sampling rate resulted in an overall duty cycle of 47% for data collection.

Absorbance measurements of the chemiluminescent solutions were also made with an absorption spectrophotometer. For purposes of comparison, the single-beam spectrophotometer had an optical geometry similar in design to that of the chemiluminescence detection instrument. The components were: a tungsten/deuterium source, a dichroic bandpass filter with a wavelength maximum equal to that of the monochromator wavelength setting, a transmission sample cell of 1 cm pathlength, an H-10 monochromator with 2 mm slits (16 nm spectral bandpass), an RCA 1P28 PMT, a current-to-voltage converter, and a digital multimeter.

Since, by their nature, many chemiluminescent reaction mixtures contain or produce fluorophores, the bandpass filter was inserted between the source and sample to reduce possible sample fluorescence interference caused by broadband source excitation. Additionally, when measuring the absorbance at the wavelength of peak chemiluminescence emission, the bandpass filter brings the source into better conformity with the spectral distribution of the chemiluminescence emission "source" used to determine the absorbance from the chemiluminescence ratio measurements. Transmittance measurements were determined as $T = (I-B)/(I_0-D)$, where I_0 is the blank signal, I is the sample signal, D is the dark signal, and B is the background signal. The dark signal, D, is the sum of the dark current and amplifier offsets, and is determined by blocking the beam between the source and the sample with the blank in place. The

background, B, is the sum of the dark signal and the chemiluminescence background, and is determined as D is, but with the sample in place. This method compensates for any interference due to chemiluminescence although the difference between B and D was only significant at absorbance values of 1 or more.

2. Reagents

Reagents were used without further purification. All solutions were prepared with deionized, distilled water, and were stored in brown glass bottles to prevent photodecomposition. The pH 9.5 buffer was 0.1 M in sodium borate and contained 0.2 mL/L of 30% Brij 35 surfactant (23). The Brij 35 wetting agent keeps bubbles which form during the course of the reaction from clinging to the cell walls. A 0.001 M solution of luminol (3-aminophthalhydrazide) (24) was prepared in 0.002 M NaOH. A 0.1 mM Mn(II) solution was prepared from $MnCl_2 \cdot 4H_2O$ (23) with dilute HCl (pH 3.0). The "activator" solution was an aqueous mixture containing 0.01 M 1,10-phenanthroline (25) with 0.1 M sodium citrate (25). Solutions that were 0.8 mM and 3.9 mM in picrate were prepared with 85% picric acid (26) in buffer with sufficient 1.0 M NaOH to restore the buffer's original pH. A 750 μM solution of ferroin (1,10-phenanthroline ferrous perchlorate) (27) was prepared in buffer.

3. Procedure

A working solution was prepared with a 2:2:1 volume ratio of the luminol, activator, and manganate standard solutions, respectively.

Before each measurement the cell was thoroughly rinsed with deionized, distilled water and aspirated to dryness. The buffer and picrate-buffer or ferroin-buffer standard solutions were then added to a combined total of 1.00 mL followed by the addition of a 0.50 mL aliquot of the working solution. A dark current measurement was made, and the reaction was initiated by the addition of a 0.20 mL aliquot of 0.1 M H_2O_2 into the cell. A 90 second delay followed to ensure complete mixing and to allow the reaction to progress beyond the lag period. Data were typically taken during a 3 to 8 minute period after which the reaction decayed to a point where the signal-to-noise ratio (SNR) became unfavorable. The logged data were transferred via a serial line to a minicomputer (28) for data reduction. The ratio, absorbance, and uncorrected and corrected intensities were reported as time-averaged values.

D. Results and Discussion

1. Choice of Chemical System

To avoid reemission errors a luminol reaction was chosen because the emitting product, 3-aminophthalate, exhibits low excitation-emission spectral overlap (29). It was also desirable for the selected luminol reaction matrix to exhibit a low absorption profile across the wavelength region of interest. The specific buffer, oxidant, and activators used provided good intensity while allowing an unusually long half-life for the luminol reaction (30). The exact reaction mechanism for this system is unknown, however, general equations are given below (31-33):

$$M + H_2O_2 \rightarrow M\text{-}H_2O_2$$

$$M\text{-}H_2O_2 + OH^- \rightarrow M\text{-}O_2H + H_2O$$

$$M\text{-}O_2H + \text{luminol} + OH^- \rightarrow \left[M\text{-}O_2\text{-luminol}\right] + H_2O$$

$$\left[M\text{-}O_2\text{-luminol}\right] \rightarrow N_2 + \left[\text{3-aminophthalate}\right]^*$$

$$\left[\text{3-aminophthalate}\right]^* \rightarrow \text{3-aminophthalate} + h\nu,\ \lambda_{max} \simeq 425\ nm$$

The long emission decay time permitted the time period in which a single intensity ratio was measured (1/2 second) to be negligibly small relative to the rate of change of the observed intensity. The SNR was also enhanced through the use of signal averaging made possible by the long reaction time. A disadvantage of the chemical system is that during the course of the reaction a chromophore of undetermined structure is formed which has an absorbance peak that tails into the region of interest. At the wavelength of peak emission (425 nm), this leads to dynamically changing absorbance values that rise rapidly from 0.00 at the beginning of the reaction and approach 0.05 toward the end of the reaction, as shown in Figure 2-4. Fortunately, these absorbance changes were near or below the limits of detectability, and the dynamic aspect of this problem was therefore inconsequential.

For purposes of testing the technique, chromophoric reagents were added to the luminol solutions to vary the matrix absorbance in the region of luminol emission. Picrate and ferroin were chosen for their

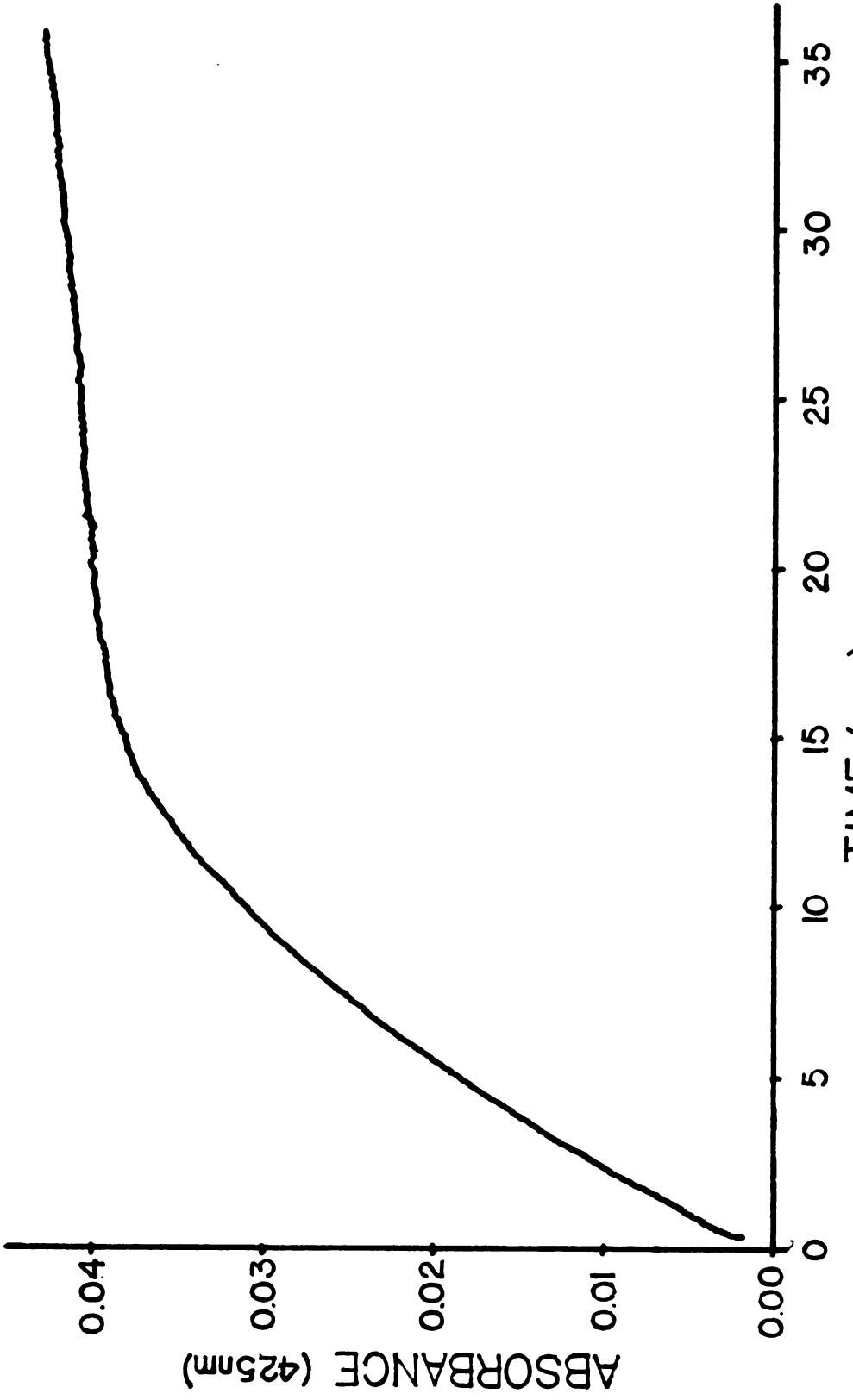

Figure 2-4. Increasing absorbance of luminol reaction matrix with time.

relative chemical compatability with the reaction matrix and for the overlap of their absorption spectra with the luminol emission spectrum, as shown in Figure 2-5. Many other chemicals were tested, however, none were found to have appropriate spectral and solubility qualities at high pH, combined with inertness to hydrogen peroxide oxidation.

In addition, other chemiluminescent chemical systems were investigated. The peroxyoxalate reaction (34,35) resulting in a chemically excited 9,10-disubstituted anthracene derivative was initially used. This reaction is extremely bright; however, it is not readily adaptable to aqueous solutions, making it inconvenient to use. Also, many of the efficient fluorophores used in the peroxyoxalate reaction have strongly overlapping excitation and emission spectra.

2. Determination of Sample Absorbance

Experiments were performed to determine the extent of agreement between absorbance values measured by a conventional transmittance technique and those derived from the chemiluminescence ratio instrument. This information also provided calibration curves to evaluate the adherence to Beer's law by both techniques. Picrate and ferroin were added in known amounts to the reaction mixture. After chemiluminescence ratio measurements the solutions were promptly transferred to the single-beam spectrophotometer where the transmittance was measured. Both instruments were set at 425 nm, the wavelength of peak luminol emission. These experiments indicated some initial disagreement between the two sets of absorbance values

Figure 2-5. Spectral distributions: luminol emission (arbitary units, solid line, right ordinate); picrate absorbance (dashed line, left ordinate); ferroin absorbance (dotted line, left ordinate).

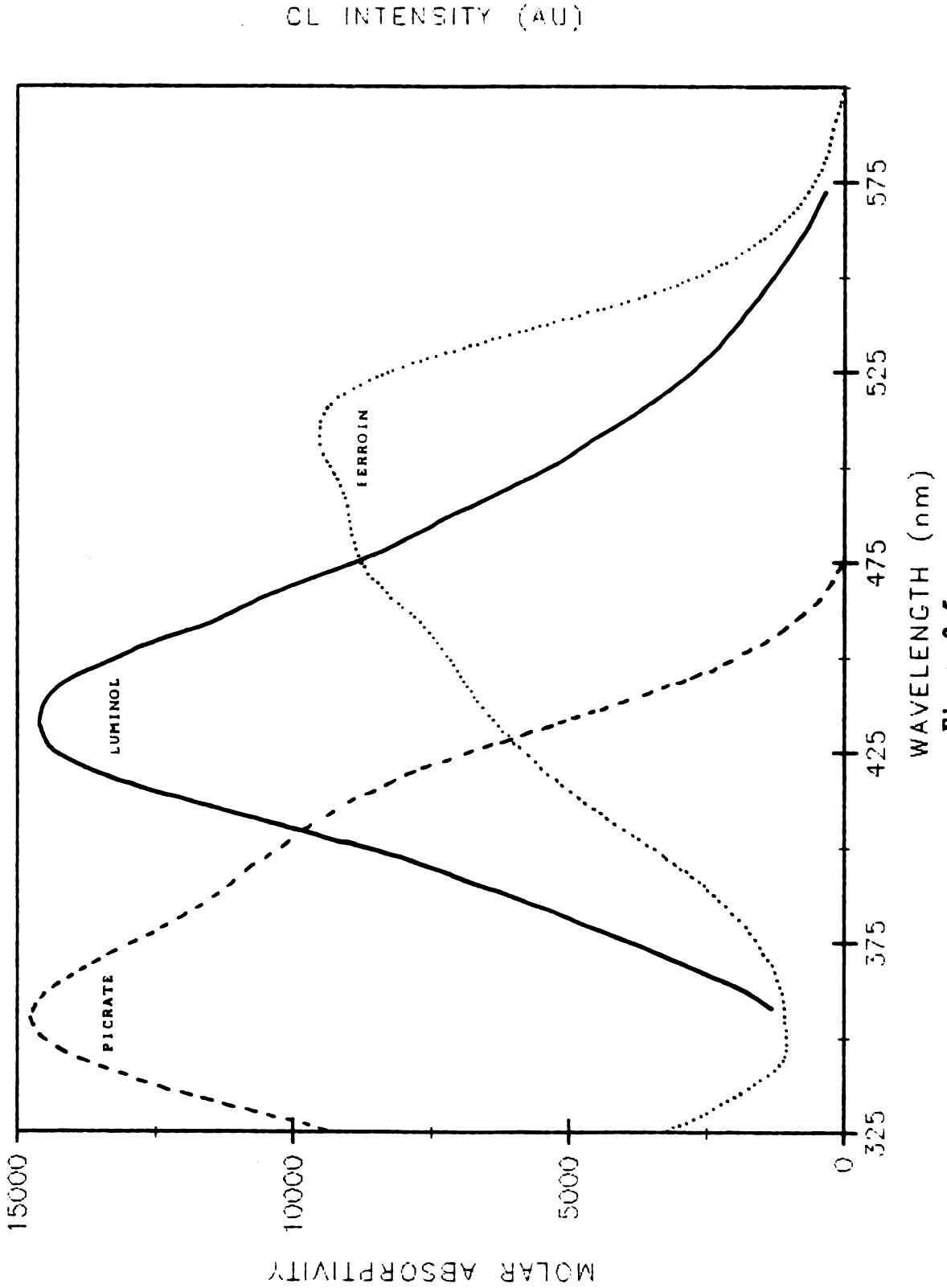
CL INTENSITY (AU)
MOLAR ABSORPTIVITY
15000
10000
5000
0
325
375
425
475
525
575
WAVELENGTH (nm)
LUMINOL
FERROIN
PICRATE

Figure 2-5

determined by the two instruments. This was attributed to the sensitivity of the ratio model to small errors in the pathlength values taken for calculation of the absorbance, and an inability to directly measure these distances accurately using conventional tools. Useful pathlength values were subsequently calculated with a non-linear curve-fitting routine, KINFIT4 (36,37). Values of R were regressed on transmittance-derived εc values taken from the linear portions of the concentration curves, in a weighted fit of Equation 2-7.

Cell pathlength values mechanically measured before mounting the cell window and values obtained by curvefitting are given in Table 2-1. Good agreement between fit values for the two data sets is observed. Fit values are somewhat larger than values predicted from the pre-assembly figures, by factors of 5.2% and 3.8% for the short and long paths, respectively. This results in a ratio of $b' : b$ that is 1.0% larger than for the measured values.

We suggest two factors which may contribute to increases in the predicted pathlengths. An actual increase in the cell pathlengths may be the result of a displacement of the cell window from its seat, caused by a thin layer of silicone sealant and elastic pressures produced in press-fitting the window into the Delrin. Alternately, the longer pathlength obtained from curvefitting may be a compensation for shortcomings in the performance of the optical system, i.e., the collimator and monochromator. To test the collimation assumption, the aperture function of the collimator was calculated in terms of its mathematical counterpart - the cylinder. A narrow cylinder appears to be an effective collimator in that it passes a relatively constant

TABLE 2-1. Comparison of pathlength values[a]

Source	# Pts	b', cm	b, cm	R[b]	r[c]
pre-assembly		0.507 ± 0.005	1.017 ± 0.005		
picrate data	11	0.536 ± 0.008	1.06 ± 0.02	0.992	0.9972
ferroin data	10	0.531 ± 0.008	1.05 ± 0.02	0.986	0.9988
combined data	21	0.533 ± 0.005	1.06 ± 0.01	0.989	0.9982

[a]Uncertainties are ± 1 standard deviation.

[b]Multiple linear correlation coefficient from KINFIT4.

[c]Linear correlation coefficient resulting from linear weighted regression, with absorbance from transmittance as the independent variable, and absorbance from CL ratio as the dependent variable.

amount of light from each emitting plane normal to the cylinder axis, irrespective of depth into the cell. According to numerical analysis of the cylinder aperture function, the amount of light from each emitting plane normal to the cylinder axis passing through the collimator increases as a function of depth into the cell. For a cylinder of dimensions equal to those of the collimator used, the relative change from the front to the back of a 1.0 cm cell is found to be approximately +4.0%. The change as a function of depth into the cell is approximately linear. The collimator was also tested experimentally by approximating an homogeneous emission plane with a selection of diffusing plates backlighted by various sources. Results varied, indicating that the collimation was effective to within approximately ± 2%. However, it appears possible that systematic errors of unknown magnitude exist in this method of collimation evaluation.

A new model was derived for the ratio of intensities by assuming a linear change with depth of the amount of light observed through the collimator. This model was then used for some KINFIT4 estimates. With 4.0 %/cm as the change in the aperture function, new values of b = 4.91 ± 0.11 mm and b' = 9.33 ± 0.24 mm were obtained. By allowing KINFIT4 to assess the collimator deviation, the values of -8.9 %/cm deviation in the aperture function with b' = 5.11 ± 0.13 mm and b = 10.21 ± 0.25 mm were obtained. Forcing the collimator deviation to be positive, as indicated by the cylinder modeling, results in a collimator aperture function deviation value of +2.8 %/cm, and pathlength values of b' = 5.26 ± 0.06 mm and b = 10.26 ± 0.15 mm. These data clearly indicate that small deviations

from ideality in the collimator function can result in substantial changes in the pathlength derived by curve fitting. However, within the experimental error of this study, curve fitting does provide a means of compensation for these unknown deviations.

The cylinder model does not account for the problem of slight internal reflections within the collimator. Reflections and scattering can and do occur within the rest of the optical system as well. The overall aperture function is also complicated by the refraction of the chemiluminescence rays as they pass through the solution/cell window/air interfaces. This effect is a result of the differences in the refractive indices of the three media and is of undetermined significance. Although it is difficult to predict the combined effects and importance of these optical non-idealities, it is possible that they cause a slight but perceptible change in R values, resulting in modified pathlength values as derived by curve fitting.

Absorbance values were then calculated using the chemiluminescence ratio and the transmittance data. The resulting concentration plots are shown in Figure 2-6. Non-zero intercepts are a result of the background absorbance produced during the reaction, as discussed earlier. Also noteworthy are the negative Beer's law deviations observed in the transmittance data at higher absorbance values. These deviations are a predictable result of the 16 nm spectral bandpass needed to ensure a useful SNR. Good correlation occurs between the chemiluminescence ratio and transmittance data for moderate absorbance values up to approximately 0.75, as shown in Figure 2-7. However, in the region of high absorbance, a positive deviation of the chemiluminescence ratio data with respect to the

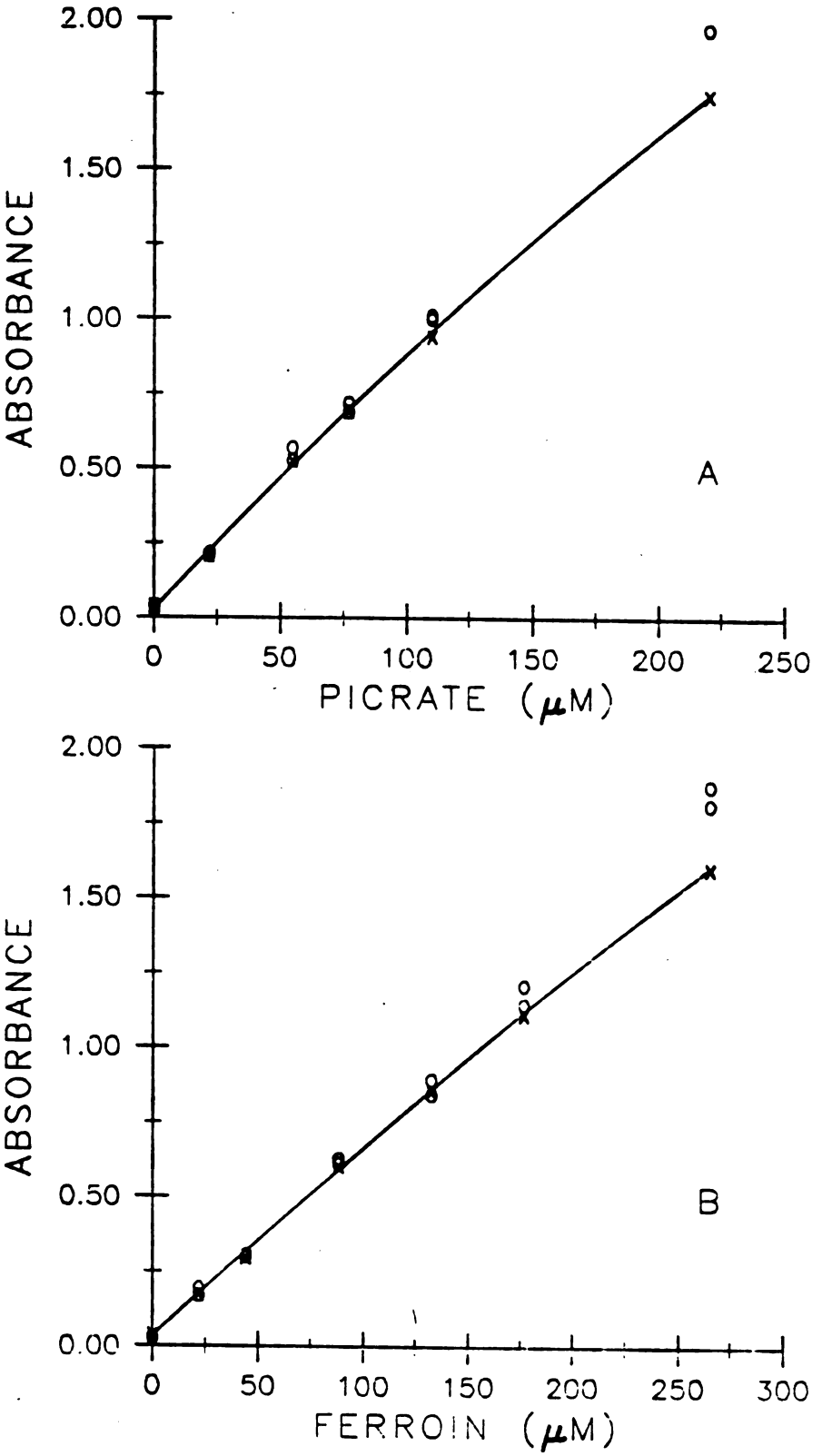

Figure 2-6. Absorbance as a function of chromophore concentration from (X) transmittance measurements and (O) CL ratio measurements.

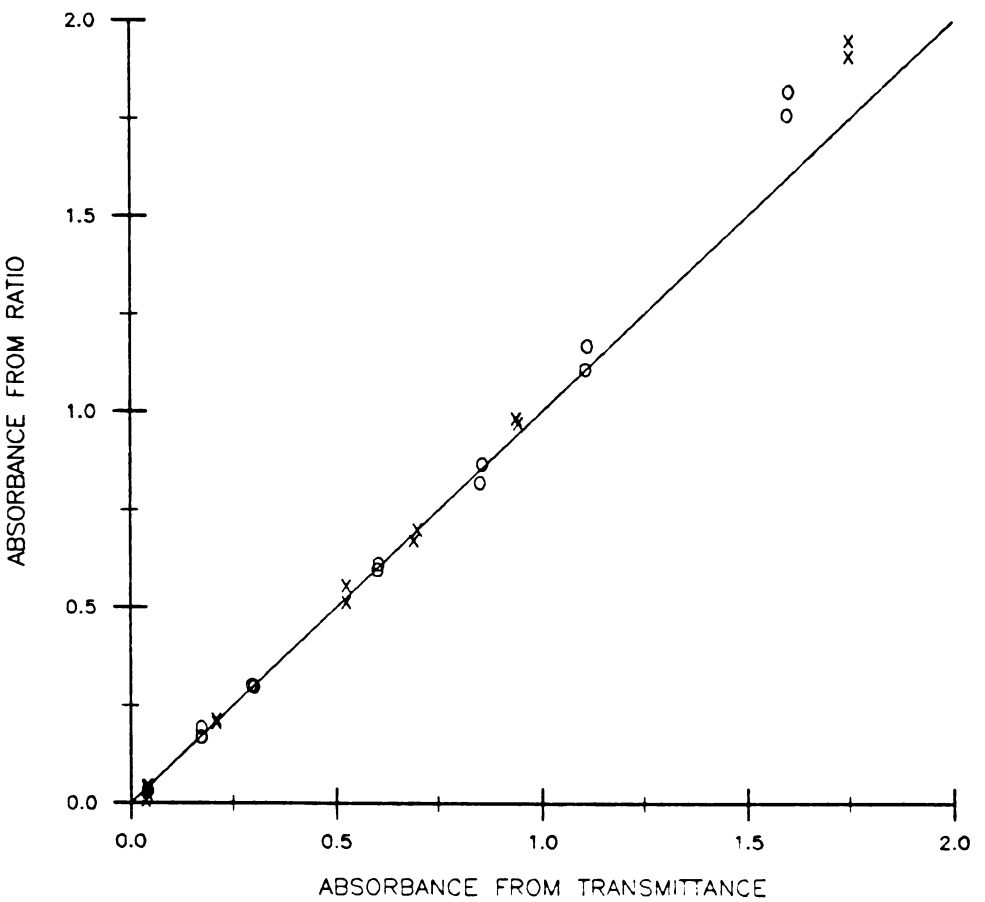

Figure 2-7. Correlation of absorbance values determined by transmittance and ratio measurements: (O) in presence of ferroin; (X) in presence of picrate. Line has ideal slope of 1.

transmittance data is observed. We have observed negative Beer's law deviations in the case of known reemission errors using other chemistries and in the case of a grossly non-monochromatic stray light situation (zero-order monochromator setting). Because of these experiences and the studies of the collimator deviations as previously discussed, the collimator was again considered as a possible source of this error. Calculations of absorbance were made using the chemiluminescence ratio equations modified to account for a small increase in light collection with depth, as observed for ideal cylinders. High absorbance values were recalculated with each set of the collimator deviation, b' and b values mentioned earlier. New values were all approximately the same or slightly higher than older values. It appears that cylinder modeling cannot explain the positive deviations found in the chemiluminescence absorbance calculations. Apparently the non-ideal behavior is a different artifact of the optical system, which becomes more pronounced in the high absorbance region.

3. Effectiveness of Correction Procedure

The conclusive test of the instrument was an evaluation of the effectiveness of the correction algorithm. Picrate and ferroin again served as chromophores. In Figures 2-8(a) and 2-8(b), attenuated and corrected intensities observed at 425 nm from the long-path side of the cell are plotted as a function of increasing picrate and ferroin concentrations, respectively. The effectiveness of the instrument in recovering effects otherwise masked by absorbance is demonstrated by

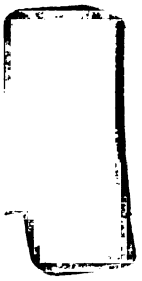

Figure 2-8. CL intensity as a function of chromophore concentration. (X) Inner-filter effect attenuated. (O) Absorption-corrected. Absorbance axis is an approximate scale for reference purposes.

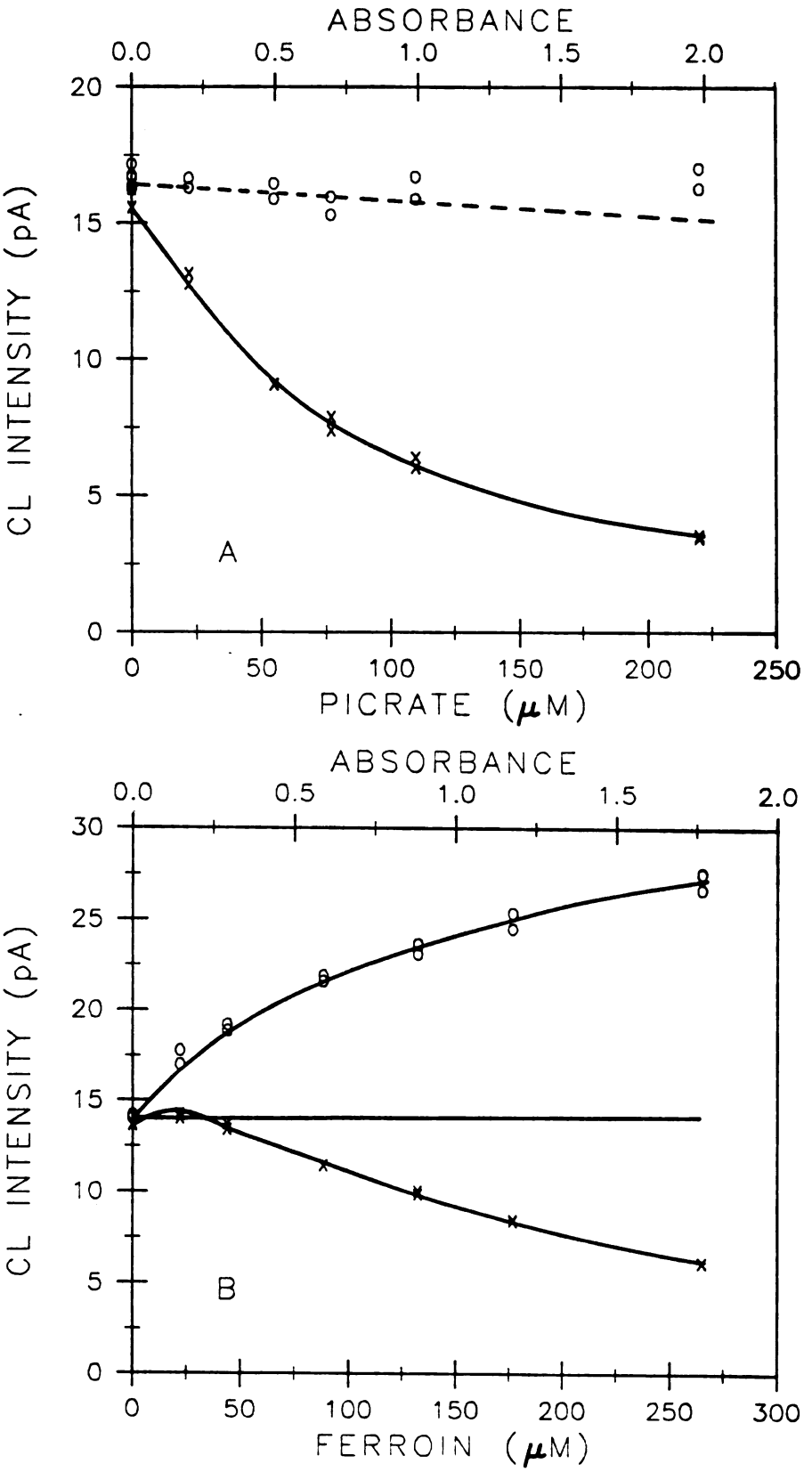
ABSORBANCE
0.0
0.5
1.0
1.5
2.0
CL INTENSITY (pA)
20
15
10
5
0
A
0
50
100
150
200
250
PICRATE (μM)
ABSORBANCE
0.0
0.5
1.0
1.5
2.0
CL INTENSITY (pA)
30
25
20
15
10
5
0
B
0
50
100
150
200
250
300
FERROIN (μM)

Figure 2-8

the difference between the corrected and uncorrected curves. Without correction, ferroin would appear to be a mild chemiluminescence activator in concentrations up to 25 μM, but a strong quencher at concentrations above 50 μM. Such results are incongruous and difficult to chemically justify, however, after correction for absorbance attenuation ferroin is demonstrated to have an increasing activation effect with increasing concentration. Picrate, too, would appear to be a strong quencher, but absorbance-correction shows this effect to be much weaker than one might originally conclude. However, the anomalously high absorbance values found above approximately 0.75 (Figures 2-6 and 2-7) translate into slightly over-corrected and possibly misleading intensity values. Experiments at 475 nm with concentrations up to 2 mM, but absorption values below 0.5, have confirmed the increasing quenching of picrate with increasing concentration, while pointing out the over-correction problem at 425 nm for picrate concentrations greater than 75 μM, as can be seen in Figure 2-8(a). Further experiments at other wavelengths have shown the same concentration dependence of the quenching and activation by picrate and ferroin, respectively, and validate the wavelength independent nature of the correction method.

The mechanisms by which picrate and ferroin affect this reaction have not been deduced. It is known that picric acid forms monopicrates with 1,10-phenanthroline and most of its known derivatives. Since the Mn(II)-phenanthroline complex is important in the catalysis of this reaction, addition of picrate would be expected to quench or otherwise perturb the catalytic mechanism. As regards the ferroin perchlorate activation, the chemical system was found to

be unaffected by the presence of the perchlorate anion alone. It was also found that ferroin had no enhancement effect in the absence of Mn(II). This suggests that the enhancement effect of the ferroin addition is due in some way to an interaction of the Mn(II) and Fe(II) phenanthroline complexes.

A corrected spectrum of the luminol emission in the presence of 90 μM ferroin was reproduced by measuring the chemiluminescence of solutions with and without ferroin at one wavelength, and similarly repeating this procedure at other wavelengths. A reference spectrum of the luminol emission, corrected for the small matrix-generated absorbance, is shown in Figure 2-9 with the uncorrected and corrected spectra of luminol emission in the presence of ferroin. Also shown is the absorption spectrum of ferroin and the matrix, generated by the correction algorithm from the same data. The uncorrected emission spectrum is misshapen and diminished in intensity by a non-constant, wavelength-dependent factor in comparison to the reference spectrum. However, the absorption-corrected spectrum has a spectral distribution identical to that of the reference spectrum, and is, by a constant factor, more intense due to activation or catalysis of the reaction.

E. Conclusions

Although the current theory requires collimation of the observed light, this constraint was initially chosen for mathematical and conceptual simplicity. A method which reduces or eliminates the collimation requirement, allowing more efficient light detection, could be similarly effective. Unfortunately, the mathematical

Figure 2-9. Luminol emission spectra (arbitrary units, left ordinate) and ferroin absorbance spectrum (right ordinate). (O) Luminol emission reference spectrum. (X) Emission spectrum attenuated by inner-filter effect due to ferroin absorbance. (#) Absorption-corrected emission spectrum. (A) Ferroin absorption spectrum from R values.

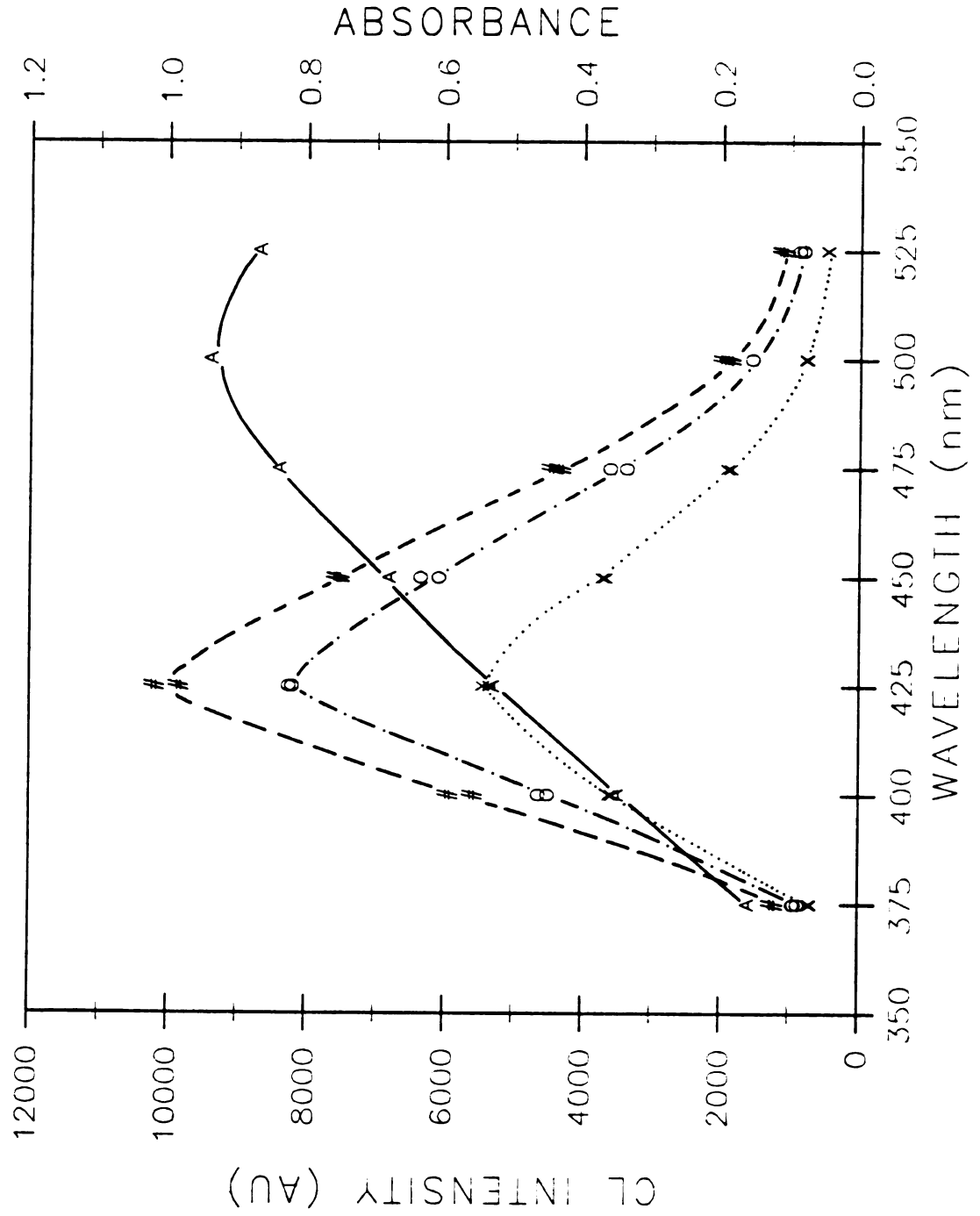
ABSORBANCE
1.2
1.0
0.8
0.6
0.4
0.2
0.0
CL INTENSITY (AU)
12000
10000
8000
6000
4000
2000
0
350
375
400
425
450
475
500
525
550
WAVELENGTH (nm)

Figure 2-9

solution for such a model is much more complex. A procedure for the evaluation of detector geometries has been suggested as a basis for extension to include self-absorption effects (38).

Further instrumental work in this area should be directed toward increasing the SNR by increasing the optical speed, devising methods for faster measurements, and studying the effects of various bandpasses and Beer's law deviation conditions. It would also be useful to incorporate a chemical system which has no background absorbance, and to find and apply chromophores which do not otherwise quench, activate, or interact with the chemiluminescence.

CHAPTER III

A FIBER-OPTIC INTERFACED FLOW CELL FOR SIMULTANEOUS ABSORBANCE AND PRIMARY INNER-FILTER EFFECT CORRECTED FRONT SURFACE FLUORESCENCE MEASUREMENTS

A. Introduction and Historical

Fluorescence techniques have become popular in analytical chemistry principally because of their sensitivity, selectivity, and wide dynamic range. These features depend on the absorbance and ensuing emission of photons at characteristic wavelengths, and with characteristic probabilities, i.e. excitation and emission spectral distributions, molar absorptivity, and quantum efficiency are all constant. As the concentration of a given analyte changes, the aforementioned characteristics should be experimentally apparent, as long as the solution absorbance at the wavelength of interest remains diminishingly small. However, if the solution absorbance at the excitation or emission wavelength does become appreciable, the excitation or detection probabilities is correspondingly diminished, which results in errors. Such errors are referred to as inner-filter effects. The inner-filter effect at excitation wavelengths is due to 'primary' absorption and likewise, 'secondary' absorption occurs at the emission wavelength.

Although fluorimetry is useful for the determination of a vast number of analytes such as blood and urine components of clinical interest, trace metals and pollutants in natural waters, and

polyaromatic hydrocarbons in petroleum products, inner-filter effects often preclude the direct use of fluorescence methods without prior separation, dilution, or derivatization steps. Especially disconcerting is the fact that many inner-filter effect errors go unnoticed because most fluorescence instruments cannot correct or even diagnose this error automatically.

Various methods have been proposed to reduce the errors caused by inner-filter effects, but many lack general applicability or suffer from various limitations. The most popular method of reducing the error is by sample dilution (39). Absorbance is reduced by dilution, but fluorescence sensitivity is also reduced. Dilution can also cause various indeterminate chemical effects. Methods which reduce the effective pathlength, thus reducing the effective absorbance, include front surface geometry (40-41), microcell (42), and altered cell positioning (42). These methods do not eliminate the errors; they only serve to lessen them to some degree. Appropriate selection of the excitation and emission wavelengths can be used to reduce or eliminate inner-filter effects (42). Unfortunately, this generally causes decreased sensitivity. For certain analyses, two-photon excitation eliminates primary absorbance errors (43), however, expensive, high-power lasers are required, because the two-photon absorption cross-section is extremely small. Until such lasers become routinely available, this solution will not become generally applicable.

Correction methods for inner-filter effects and associated problems in fluorimetry have been addressed in a variety of ways for several years and continue to be of interest to many. Two excellent

references to the historical development and current state-of-the-art in correction methods can be found in the work of Christmann and Adamsons (11-13, 44-45). The only other recent addition to the literature of notable interest has been a semi-empirical method of correcting for primary inner-filter effects in synchronous fluorescence spectrosopy (46).

The major portion of the work on absorption-corrected fluorescence has centered on methods for right-angle instruments, since most commercial instruments use right-angle detection. Most of the remaining methods are for the determination of quantum efficiencies, for which a variety of configurations have been suggested. No attention has been directed to applications involving flowing streams, and little interest in small volume techniques has been expressed. This technological gap has led to the development of the fiber optic coupled, small volume flow cell for front surface, primary absorption-corrected fluorescence, as presented here.

Mitchell, Garden, and Aldous (40) introduced a front-surface fluorescence instrument which uses a bifurcated fiber-optic to achieve a front surface fluorescence geometry. Smith, Jackson, and Aldous (48) went on to develop a flow cell based on this technology. The "Y"-shaped bifurcated fiber optic is used to direct the excitation beam into one arm of the "Y" to excite fluorophores at the common end. Emitted light returns from the common end through the second arm of the "Y" where it may be detected. In this way, the bifurcated fiber optic simplifies front surface (zero degree) fluorescence detection. Errors due to inner-filter effects are reduced with front surface fluorescence as compared to right angle fluorescence because the

effective pathlengths are shorter. Since the common end of a bifurcated fiber optic may be used as the front cell window (or immersed in the solution) an efficient, large solid angle is formed for both excitation and for observation of emission, and the reflection of excitation light from the cell window back to the detector, a problem with other 0° techniques, is eliminated. In addition, the fiber optic input/output characteristics are almost independent of length, causing the input and output to appear optically as though they were spatially the same, i.e., as though the fiber optic was vanishingly short. This simplifies optical layout and alignment, and optimizes the efficiency of light transport.

The balance of this chapter describes the theoretical development of a correction model for the bifurcated fiber optic cell. It is shown how the unique characeristics of the fiber optic as a cell window are incorporated into a volume source model of a cylindrical flow cell. The flow cell also allows transmittance measurements to be made of the fluorescence excitation beam. This information is used to calculate the inner-filter effect correction.

B. Theory

An excellent theoretical basis for quantitative signal vs. concentration or signal vs. absorbance relationships in fluorimetry is available in the work of van Slageren, et al. (47). For convenience, and because some unique differences occur for the cell modeled here, a complete derivation is given.

Consider a fluorescence cell initially having the following characteristics and conditions, as shown schematically in Figure 3-1:

1. A cylinder of known dimensions defines the volume of the cell.
2. The excitation-emission window is located at one end of the cylinder, perpendicular to the cylinder axis. It is formed by the optical face of the common leg of a bifurcated fiber optic containing the randomized fibers of both fiber bundles.
3. A transparent window at the opposite end of the cell affords exit for the excitation beam, thus allowing transmittance measurements to be made.
4. The cell's windows and cylindrical wall are non-reflective.
5. Excitation and observed emission is monochromatic, homogeneous, and parallel to the cell axis.
6. Scattered light, refractive index effects and reflections within the cell are assumed to be negligible.
7. Reemission is negligible.

The radiant power P_x, at any point in the cell a distance x from the excitation window is given by Beer's law as

$$P_x = P_0[10^{-\{(\varepsilon c)_{ex}x\}}] = P_0[e^{-2.303\{(\varepsilon c)_{ex}x\}}] \qquad (3\text{-}1)$$

where $(\varepsilon c)_{ex}$ represents a summation of the absorptivities per unit pathlength at the excitation wavelength, and P_0 is the unattenuated power of the excitation beam at the window. The fluorescent radiant power generated at this point dF_{dx}, is a function of the amount of light absorbed by the fluorophore as given by

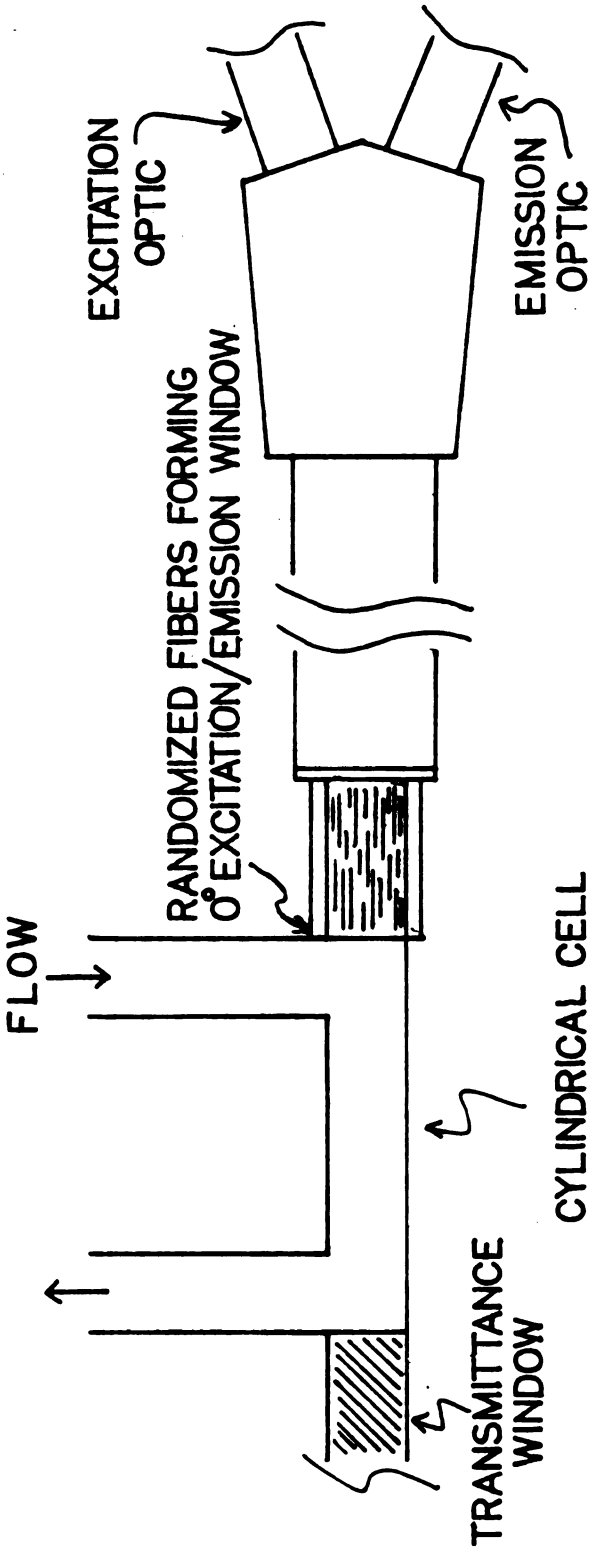

Figure 3-1. Schematic cut-away diagram of bifurcated fiber-optic fluorescence flow cell.

$$dF_{dx} = QP_x(\varepsilon c)_F dx = QP_0[e^{-2.303\{(\varepsilon c)_{ex}x\}}](\varepsilon c)_F dx \qquad (3\text{-}2)$$

where Q is the fluorophore quantum efficiency, and $(\varepsilon c)_F$ represents a summation of the absorptivities per unit pathlength of the fluorophores. The fluorescent radiant power observed from this plane dF_x, is a function of absorptivity per unit pathlength at the emission wavelength:

$$dF_x = T(x)dF_{dx}[e^{-2.303\{(\varepsilon c)_{em}x\}}]$$

$$= T(x)P_0\left[e^{-2.303\{(\varepsilon c)_{ex} + (\varepsilon c)_{em}\}x}\right](\varepsilon c)_F dx \qquad (3\text{-}3)$$

where $(\varepsilon c)_{em}$ represents a summation of the absorptivities per unit pathlength at the emission wavelength and T(x) is a transfer function that incorporates quantum efficiency, wavelength dependence and efficiencies of optics and detectors, and the fraction of light transmitted through the fiber optics as a function of depth into the cell. The total fluorescence observed F_b, is determined by integrating Equation 3-3 over the length of the cell, b:

$$F_b = P_0(\varepsilon c)_F \int_0^b T(x)e^{-2.303\{(\varepsilon c)_{ex} + (\varepsilon c)_{em}\}x}dx \qquad (3\text{-}4)$$

If the excitation and emission beams are parallel to the cell axis, T(x) may in general be considered constant and Equation 3-4 is solved simply. Unfortunately, a parallel beam requirement implies a very collimated beam and thus low excitation and emission light throughput efficiency. On the other hand, the fiber optic allows facile excitation/emission coupling with good excitation/emission efficiency. Since the fiber optic transmittance is dependent upon the

angle of incidence of the input light, the transfer function T(x) for a fiber optic must be explicitly incorporated into Equation 3-4.

Cell modeling incorporating the fiber optic angular transmittance function based on methods discussed in Chapter V indicates that the transfer function follows an exponential decay with increasing distance into the cell. This modeling assumes infinitesimally small fibers and perfectly random distribution of the excitation and emission fibers. In practice, the finite size of the individual fibers and the non-random grouping of the fibers causes the transfer function to be significantly different than that modeled for short distances from the fiber optic face. Each individual excitation fiber emits light into a volume which can be described as an inverted frustum of a cone. Likewise, each individual emission fiber collects light from a conically shaped volume. Additionally, as the angle of incidence of a transmitted ray increases from normal to the fiber face, the transmittance of the fiber decreases. The net effect results in discrete volumes being excited near the fiber optic surface from which emission cannot be observed because the cones of excitation and the cones of observation do not yet overlap. No emission is observed from the solution at the surface of the fiber optic, but as the distance from the the fiber optic face increases, the overlap of the excitation and collection cones increases until this effect becomes negligibly small. Although this effect has not been modeled on more than an intuitive level, it would seem fair to approximate such an effect roughly as an exponential increase approaching zero slope at infinite distance. By convoluting this exponential increase with distance with the exponential decay previously modeled, the

transfer function can be understood to be characterized by an initial increase from zero followed by an exponential decay from a maximum value.

Experimental evidence supporting this mathematical/intuitive description of the transfer function has been provided by Smith, Jackson, and Aldous (48). These workers measured (Figure 5, reference 48) radiation from the bifurcated fiber-optic excitation arm that backscattered from a reflective surface and was collected and detected through the emission arm. The detected scattered light intensity was found to increase with increasing distance of the reflective surface with an intensity minimum of about 10% of maximum at zero scattering distance. Maximum scatter intensity was observed with a scattering distance of 3 mm. Scattering then descreased exponentially to a low of 5% of maximum with the reflective surface 30 mm distant from the optic. An empirical mathematical description of such a function that can be exactly integrated within Equation 3-4 is

$$T(x) = G(e^{-Hx} - e^{-Kx}) \qquad (3\text{-}5)$$

where G is a normalization constant, K describes the exponential increase, and H describes the exponential decay. Each of these values can be determined by curve fitting as described later.

By substituting Equation 3-5 into Equation 3-4 and integrating, the total fluorescence observed can be described in terms of the respective absorbances within the solution by

$$F_b = P_0(sc)_F G\left[\frac{1}{M}(1-e^{-Mb}) - \frac{1}{N}(1-e^{-Nb})\right] \qquad (3\text{-}6)$$

where

$$M = H + 2.303\{(\varepsilon c)_{ex} + (\varepsilon c)_{em}\}$$

$$N = K + 2.303\{(\varepsilon c)_{ex} + (\varepsilon c)_{em}\}$$

The limiting form of Equation 3-6 for low absorbance becomes

$$F_0 = P_0(\varepsilon c)_F G\left[\frac{1}{H}(1-e^{-Hb}) - \frac{1}{K}(1-e^{-Kb})\right] \qquad (3\text{-}7)$$

where F_0 is the unattenuated fluorescence observed.

If a correction factor CF, is defined such that

$$F_0 = CF \cdot F_b$$

then by substitution of Equations 3-6 and 3-7 into Equation 3-8, and rearrangement, the correction factor is

$$CF = \frac{\frac{1}{H}(1-e^{-Hb}) - \frac{1}{K}(1-e^{-Kb})}{\frac{1}{M}(1-e^{-Mb}) - \frac{1}{N}(1-e^{-Nb})} \qquad (3\text{-}9)$$

C. Experimental

1. Reagents

All chemicals were commercially available reagents and were used without further purification, unless otherwise noted. All solutions were prepared with 0.2 N H_2SO_4. A stock solution of 10.0 mM quinine sulfate (QS) (24) was used to prepare solutions in the range of 0.1 μM to 0.4 mM. A stock solution of 40.0 mM 2,5-dihydroxybenzoic acid (DHBA) (24) (recrystallized from water) with 20.0 μM QS was used to prepare a series of DHBA solutions ranging from 0.1 to 0.8 mM with a constant concentration of 20.0 μM QS. A series of 0.1 mM to 0.8 mM

DHBA solutions was also prepared. A solution of 0.0500 g/L $K_2Cr_2O_7$ in 0.01 N H_2SO_4 was prepared for the determination of the cell pathlength (49). Nine solutions with sodium fluorescein concentrations ranging from 0.0 μM to 80 μM were made with a constant 20.0 μM QS concentration. All solutions were transferred to hard polyethylene bottles immediately after preparation to prevent adsorption losses. All solutions were stored in the dark to avoid photodecompostion.

2. Apparatus and Procedure

A schematic diagram of the fluorescence instrument is shown in Figure 3-2. To construct the sample cell, a cylinder with an inside diameter of 2.0 mm was formed from a black Delrin rod (16) having a 6.4 mm outer diameter. This was press-fit into a stainless steel block which was then machined to allow the inlet and outlet of solution at the ends of the cylinder via 2.0 mm holes perpendicular to the cell axis. The block was also machined for the mounting of the bifurcated quartz fiber optic (50) and a 2.0 mm diameter by 50 mm quartz rod (51), which act as cell windows. A 1.0 mm transmittance path is formed, creating a 32 microliter cell volume. The entrance slit of an f/3.5 UV grating monochromator (52) with a 10 nm/mm reciprocal linear dispersion is positioned to collect light from the cell through the cell's quartz window/light pipe. This monochromator is required to reject stray light and fluorescence which interfere with measurements of the transmittance of the excitation beam. A 20 nm bandpass was permitted through the use of 2.0 mm slits. A silicon photocell housing with integral amplifier is used for light detection.

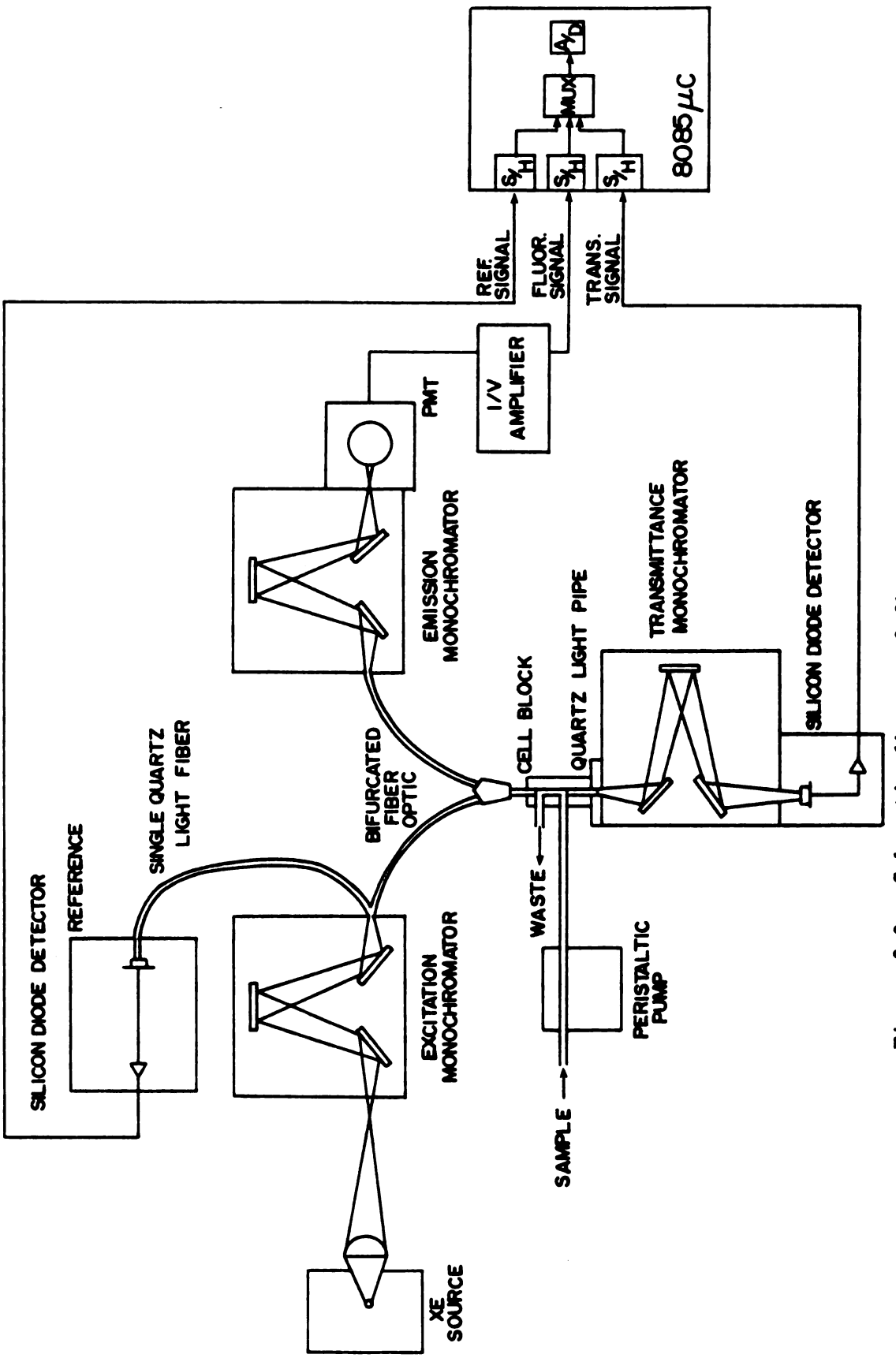

Figure 3-2. Schematic diagram of fluorescence instrument.

Solutions are continuously pumped or drawn from the cell by means of a peristaltic pump at the rate of approximately 1 mL/minute.

The excitation source is a high pressure xenon short arc lamp (150 W) driven by a constant-power lamp supply (53). The source radiation is focussed by an optically fast projection lens onto the entrance slit of an f/3 monochromator (16 nm/mm reciprocal linear dispersion) (19). The excitation arm of the bifurcated fiber-optic is placed at the exit slit. A single quartz light fiber is placed in close proximity to the excitation optic to transmit a reference beam to a silicon photocell detector (54). The reference signal required to compensate for source drift. The emission arm of the bifurcated fiber optic is centered in front of the entrance slit of a second f/3 monochromator, identical to the emission monochromator. The PMT fluorescence detector current output is converted to voltage and amplified (21) by 10^7 to 10^{10} V/A. The PMT supply voltage ranged from -500 to -650 volts.

The voltage outputs from the three detectors are simultaneously sampled at 5 millisecond intervals by synchronously triggered, differential input sample-and-hold (S/H) amplifiers. The sampled signals are then successively transferred via an analog multiplexer to a 12-bit ADC with a 35 microsecond conversion time. Average signal values are accumulated from 2000 samples and displayed in tabular form along with reference-corrected transmittance and fluorescence values.

D. Results and Discussion

1. Determination of Cell Parameters

The cell pathlength was determined by measuring the absorbance of 0.0500 g/L $K_2Cr_2O_7$ at 350 nm. The absorbance was found to be 0.5351 ± 0.0003. The absorptivity was taken as 10.71 L/cm g (48) from which the cell pathlength was fortuitously found to be 1.000 cm.

Having obtained the cell pathlength, the only other parameters required for the correction factor equation are the empirical transfer function values for H and K of Equation 3-5. In addition, freedom from stray light and fluorescence interference in the transmittance measurements must be confirmed by experimentally verifying absorbance linearity as a function of concentration. With experimental fluorescence and absorbance concentration curves of quinine sulfate (QS), the instrument may be checked for adherence to Beer's law while providing fluorescence information to test the suitability of Equation 3-5 by evaluating the goodness of fit of the data to Equation 3-6. Fluorescence and absorbance values were determined for solutions of QS ranging from 0.1 μM to 400 μM. A 4 nm bandpass (0.5 mm slits) centered at 365 nm (excitation maximum) was used for excitation and a 16 nm bandpass (2.0 mm slits) centered at 450 nm (emission maximum) was chosen for emission. The PMT voltage was -600 V and the fluorescence current sensitivity was 10^9 V/A.

Excellent absorbance linearity to greater than 3 absorbance units was observed, as shown in Figure 3-2. A weighted least squares linear regression of absorbance as a function of concentration resulted in these figures of merit:

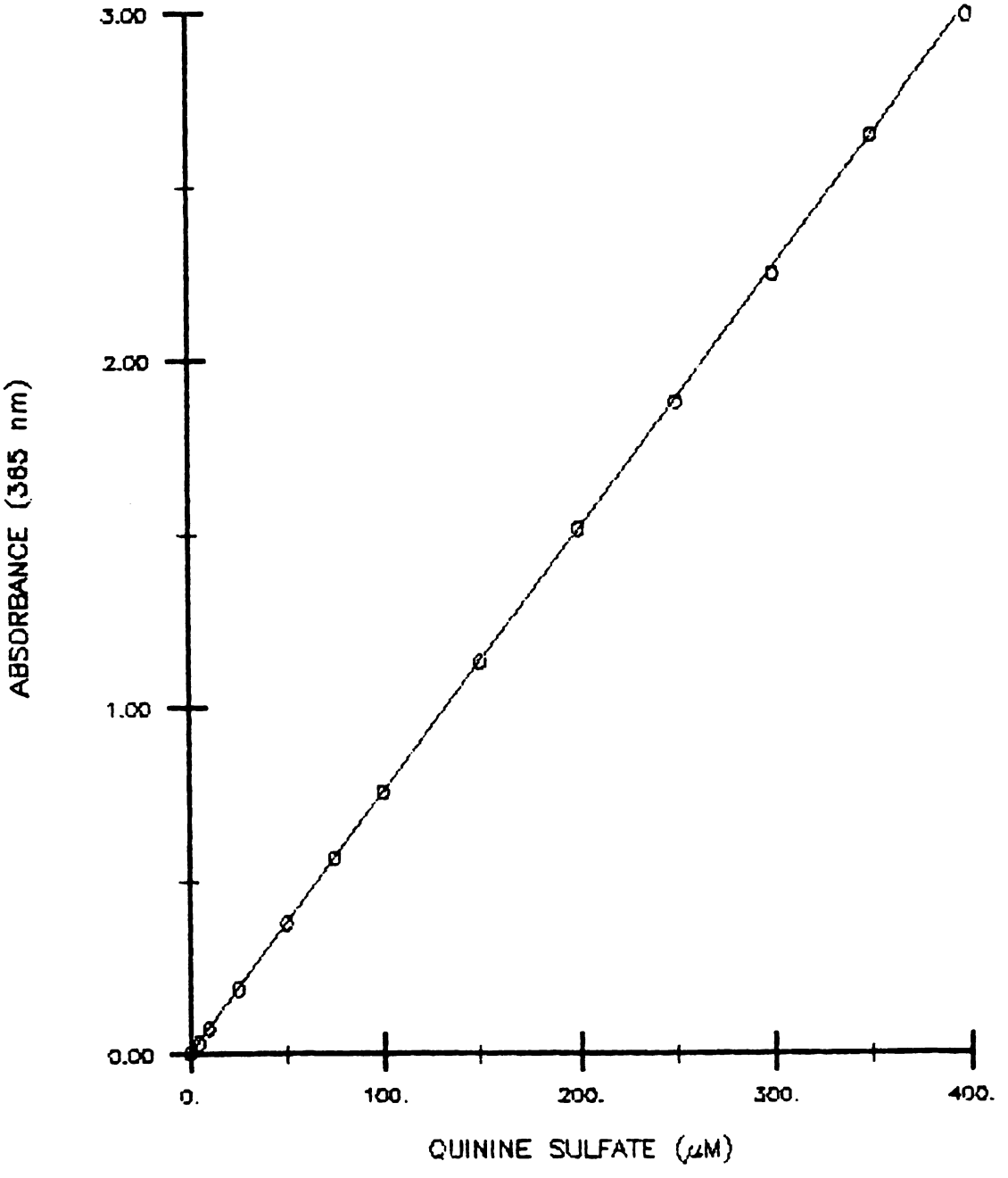

Figure 3-3. Quinine sulfate absorbance at 365 nm.

slope, (sb) = 7566. ± 3. M^{-1}

intercept = −0.0015 ± 0.0004

standard error = 0.0019

correlation coefficient, (r) = 0.9999905

Worst case linearity extends to an absorbance of 1.0 with a 16 nm excitation bandpass. Large Beer's law deviations were observed for conditions of high fluorophore concentration with highly absorbing solutions when the transmittance monochromator was removed. This problem results from the fluorescence becoming a significant fraction of the light detected by the transmittance detector. Although the need for post-cell transmittance filtering was not anticipated, the 20 nm bandpass of the transmittance monochromator was found to adequately reject fluorescence. Earlier, a broadband filter was found to be sufficient; however, the convenience of tunability with the monochromator is much more desirable.

Values of H and K were determined by regression of the fluorescence vs. absorbance ($(sc)_{ex}$) data on Equation 3-6 ($(sc)_{em} = 0$) using KINFIT4 (37,38). Excellent results were obtained:

H = 1.108 ± 0.052

K = 9.60 ± 0.33

The average relative error of the calculated estimates was 0.05%. With data from a second, repeated experiment and these estimates of the parameters H and K, primary absorbance corrected fluorescence values were calculated using Equations 3-8 and 3-9. Figures 3-4 and 3-5 show the uncorrected and corrected fluorescence data as a function of concentration in linear and logarithmic form. The corrected fluorescence is linear over nearly 4 decades. Weighted

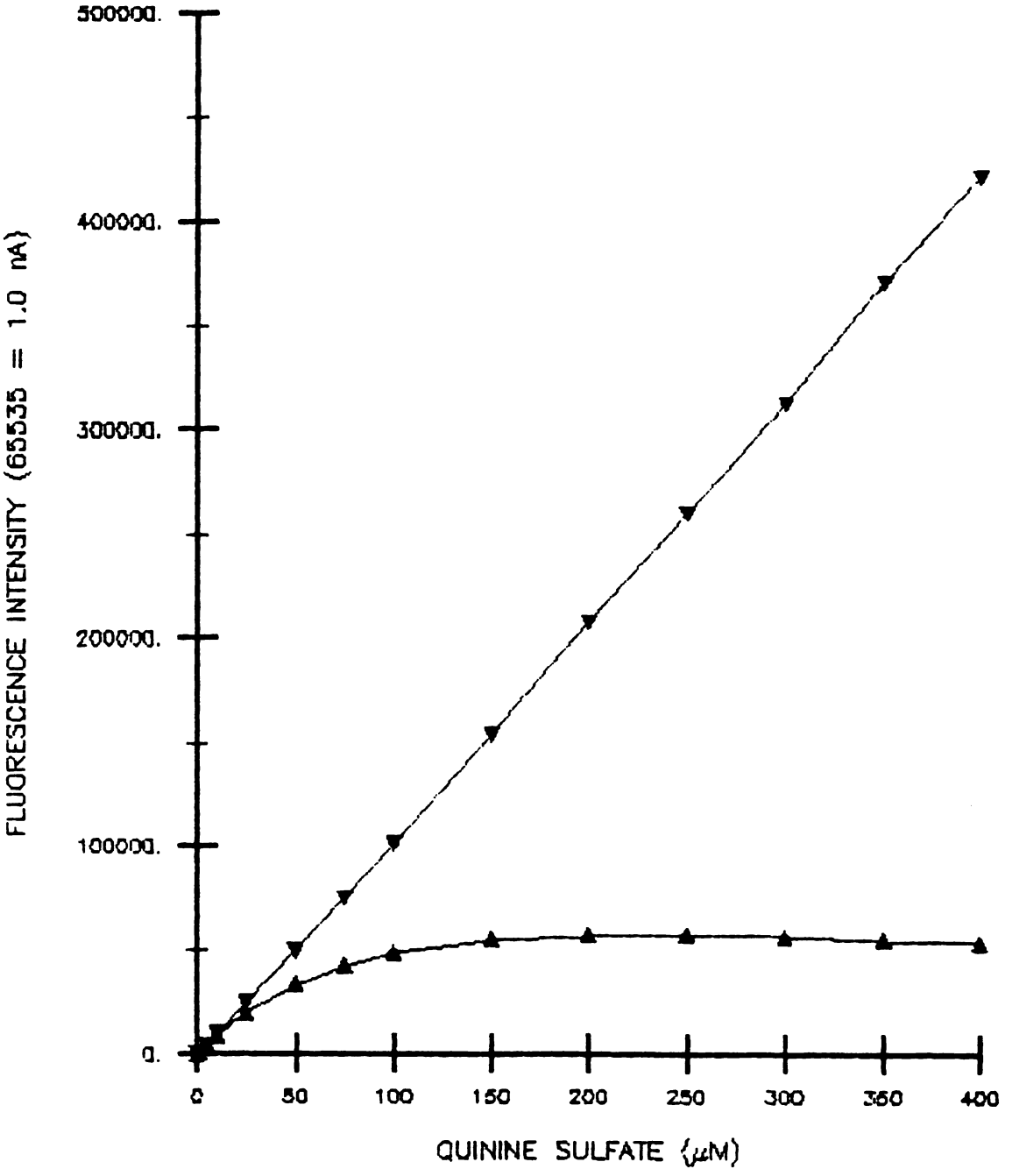

Figure 3-4. **Fluorescence intensity (65,535 = 1.0 nA PMT anode current) vs. quinine sulfate concentration; linear-linear plot. (▲) Uncorrected; (▼) Absorbance-corrected. 365 nm excitation wavelength; 450 nm emission wavelength.**

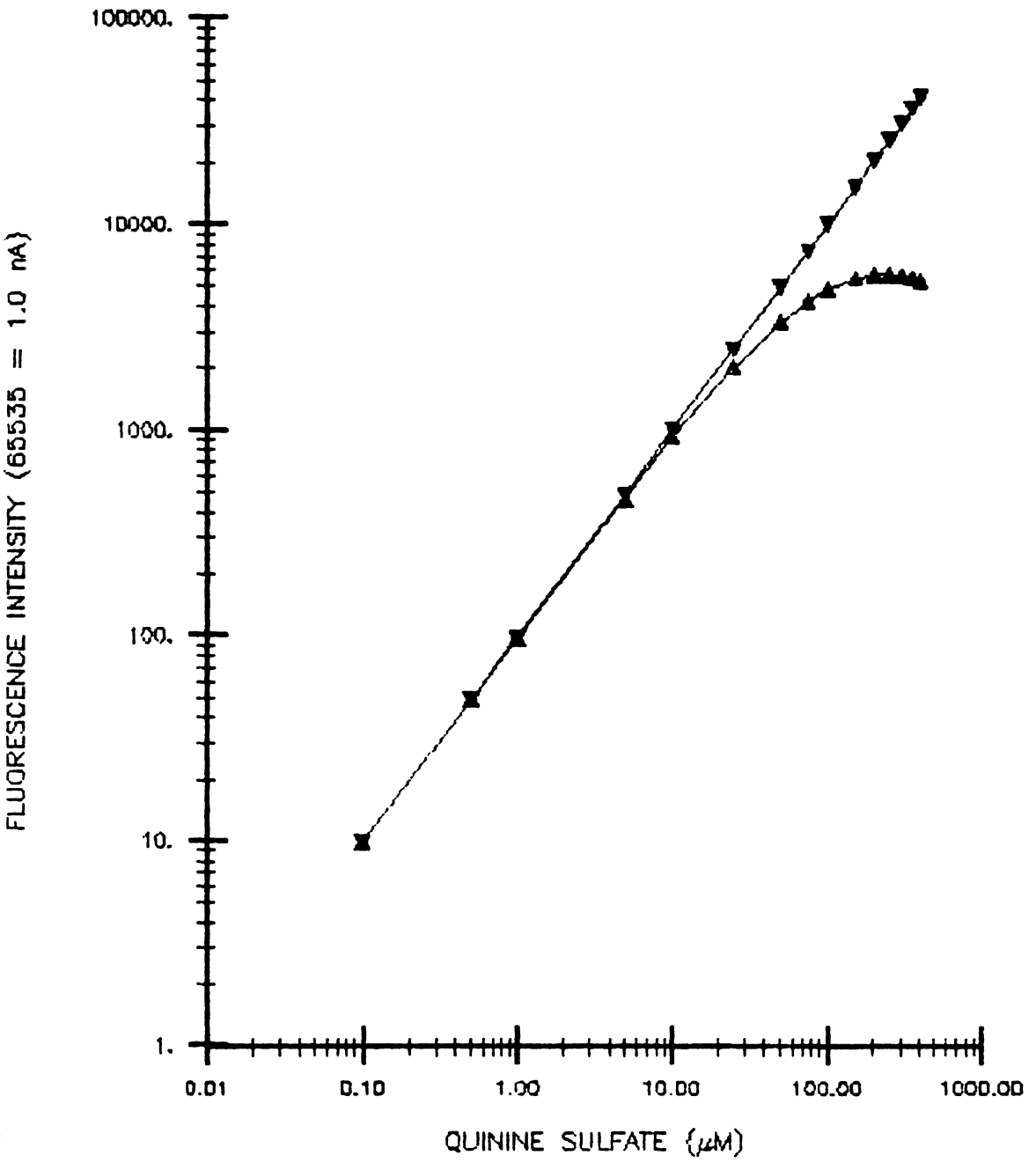

Figure 3-5. Fluorescence intensity (65,535 = 1.0 nA PMT anode current) vs. quinine sulfate concentration; log-log plot. (▲) Uncorrected; (▼) Absorbance-corrected. 365 nm excitation wavelength; 450 nm emission wavelength.

linear regression of corrected fluorescence provides the following summary:

slope = [1.02609 ± 0.00028] · 10^9 M^{-1}

intercept = -80 ± 5

standard error = 406

correlation coefficient, (r) = 0.99975

The unique properties of the bifurcated fiber-optic coupling result in a decrease in the fluorescence signal at absorbances greater than 1.5. As the absorbance increases, there is a movement toward the fiber-optic of the volume in which most of the excitation beam is absorbed, and thus, from which most of the fluorescence is emitted. As this emission volume moves very close to the fiber-optic, the emission-collection fibers are spatially precluded from efficient emission collection, as earlier predicted.

2. Effectiveness of Correction Procedures

To evaluate the effectiveness of the primary absorbance correction, 2,5-dihydroxybenzoic acid (DHBA) was used as an interfering chromophore. The absorption spectrum of DHBA in 0.2 N H_2SO_4 has a peak at 329 nm which falls off to zero above 400 nm. At pH values higher than 2.0, DHBA fluoresces strongly in the blue region. However, in 0.2 N H_2SO_4 (pH ≃ 1.0) the quantum efficiency decreases dramatically (55). Fortunately, DHBA does not quench the QS fluorescence, nor does the fluorescence spectrum of DHBA overlap appreciably with the excitation spectrum of QS; thus any error due to reexcitation and reemission via this pathway is precluded.

An experiment was devised by which the QS fluorescence at constant concentration was to be determined in the presence of varying amounts of the primary-absorbing and fluorescing DHBA. One set of solutions was prepared with 20.0 μM QS and 0.0 mM to 0.8 mM DHBA in 0.2 H_2SO_4. Another set of solutions was prepared with matching concentrations of DHBA in H_2SO_4, but without QS. Using a 4 nm excitation bandpass centered at 329 nm, the DHBA absorbance maximum, and a 16 nm emission bandpass centered at 450 nm, the QS emission maximum, both sets of solutions were examined. The PMT voltage was -610 V, and the current-to-voltage converter was maintained at 10^9 V/A gain. Absorbance values extended to 3.25 with good linearity. The absorbance-corrected fluorescence intensity from QS was determined by subtracting the corrected fluorescence contribution of the DHBA, as determined from the DHBA solutions, from the corrected fluorescence intensity of the mixed QS and DHBA solutions. The results are shown in Figure 3-6, amply demonstrating that the technique accurately corrects for primary-absorbance inner-filter effects. The average relative standard deviation of the mean QS fluorescence is 0.39%, while the maximum error is less than 1%.

Since the QS also contributes appreciable primary absorbance (A = 0.17), the experiment demonstrates that the correction technique is independent of the number of fluorophores or the relative distribution of absorbance between principle fluorophore and other chromophores, while validating the additivity of corrected fluorescence.

Figure 3-6. Quinine sulfate (QS) and 1,5-dihydroxybenzoic acid (DHBA) fluorescence intensity (65,535 = 1.0 nA PMT anode current):
(■) Primary-absorbance attenuated and
(□) absorbance-corrected fluorescence from 20.0 μM QS with 0.0 to 0.8 mM DHBA;
(▲) Primary-absorbance attenuated and
(▽) absorbance-corrected fluorescence from 0.0 to 0.8 mM DHBA;
(X) Absorbance-corrected fluorescence of 20.0 μM QS in the presence of 0.0 to 0.8 mM DHBA, DHBA fluorescence subtracted: X = □ - ▽ .
328 nm excitation wavelength; 450 nm emission wavelength.

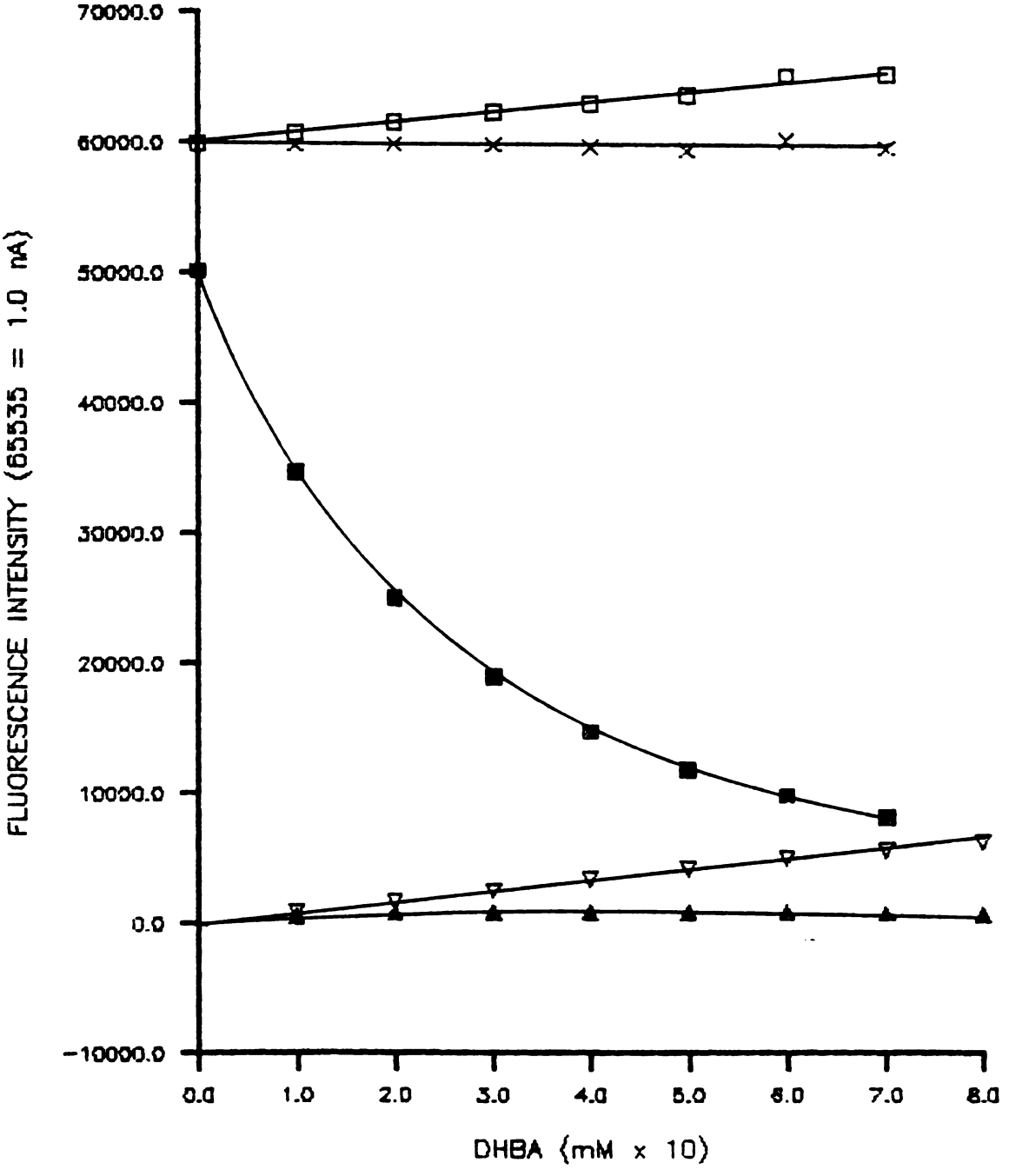
70000.0
60000.0
50000.0
40000.0
30000.0
20000.0
10000.0
0.0
-10000.0
FLUORESCENCE INTENSITY (65535 = 1.0 nA)
0.0
1.0
2.0
3.0
4.0
5.0
6.0
7.0
8.0
DHBA (mM x 10)

Figure 3-6

3. Effectiveness of Correction for Secondary Absorbance

Although this instrument was not initially designed or intended for correction of secondary absorbance inner-filter effects, the method, as derived, is theoretically capable of including both primary and secondary absorbance in the correction factor. To test this hypothesis, the secondary absorbance-corrected fluorescence of 20.0 μM QS was determined in the presence of 0.0 μM to 80.0 μM sodium fluorescein in 0.2 N H_2SO_4. The excitation and emission wavelengths were 365 nm and 438 nm (fluorescein absorbance maximum), respectively, and both monochromators had 4 nm bandpasses. The narrow excitation bandpass is necessary to maintain Beer's law linearity for absorbance measurements and the emission bandpass is adjusted to match the bandpass at which the absorbance is determined. The excitation and transmittance monochromators were first set at the emission wavelength of 438 nm and the secondary absorption was measured for all solutions. The excitation and transmittance monochromators were then reset to the excitation wavelength. The primary absorbance at 365 nm and fluorescence at 438 nm were then measured for all solutions. The primary absorbance ranged from 0.16 to 0.33 while the secondary absorbance ranged from 0.00014 to 3.06, with good linearity. The fluorescence values were corrected for both primary and secondary absorbance inner-filter effects. Results are shown in Figure 3-7. The relative standard deviation of the mean corrected fluorescence is 1.5%. However, all of the results appear to be high relative to the first solution which had negligible secondary inner-filter attenuation, since it contained no fluorescein. Relative to the first

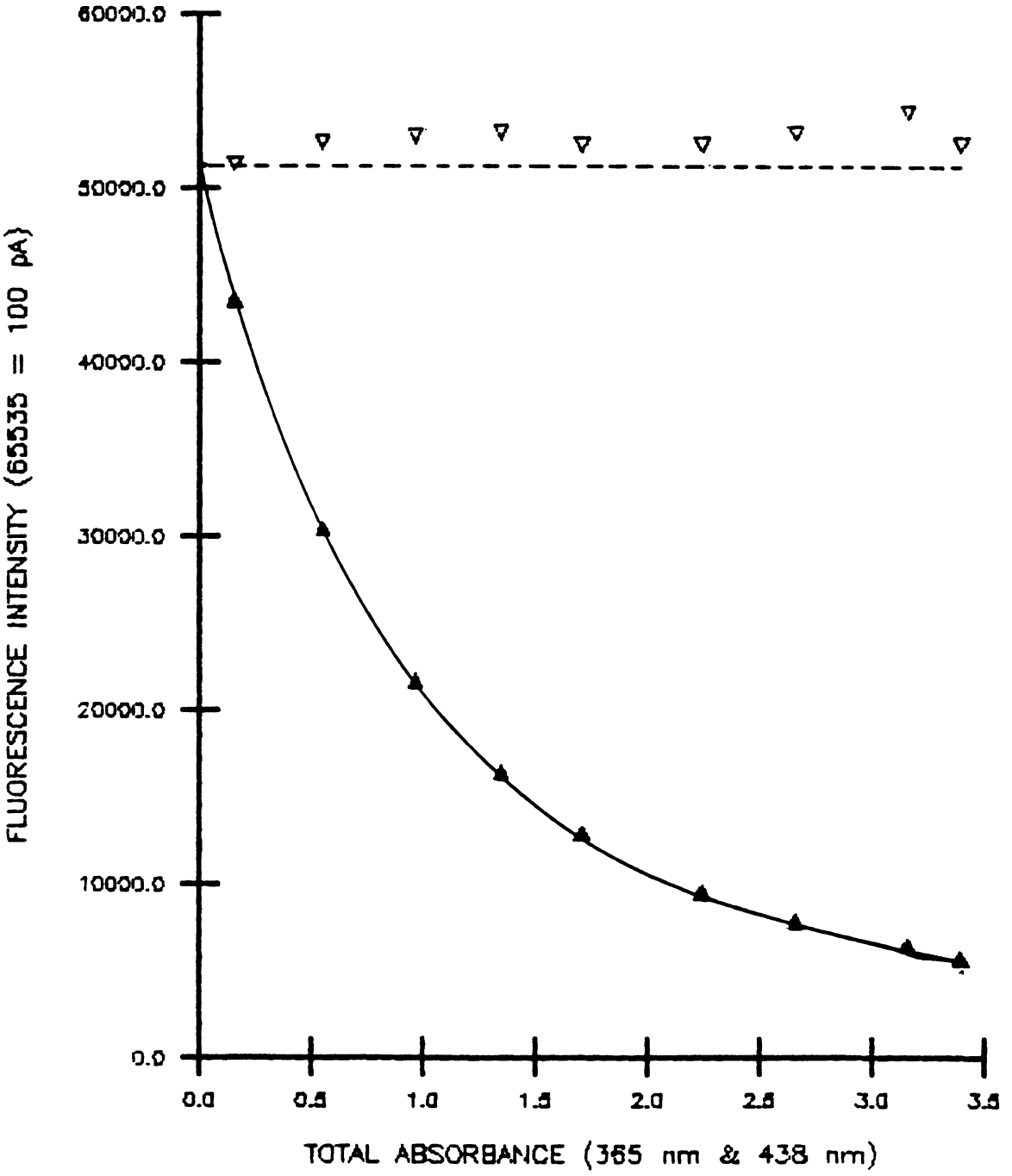

Figure 3-7. Fluorescence intensity (65,535 = 100 pA PMT anode current) vs. total absorbance of 20.0 μM quinine sulfate in the presence of 0.0 to 80.0 μM sodium fluorescein: (▲) Uncorrected; (▽) Primary and secondary absorbance-corrected. 365 nm excitation wavelength; 438 nm emission wavelength.

solution, the mean error is 3.1%, and the largest error is 6%, which is much improved compared to the range of errors of 41% to 89% before absorbance correction.

Several potential problems could contribute to the positive errors. The wavelength setting accuracy of the excitation and emission monochromators is ±1 nm and the setting reproducibility is ± 0.4 nm. A significant discrepancy between the wavelength at which the absorbance was actually measured and the wavelength at which the fluorescence was measured could have contributed to an error. Secondly, although the quantum efficiency of fluorescein in acid is low, a small overlap of the fluorescein fluorescence spectrum at 438 nm could cause a slight additional fluorescence contribution. This possibility seems unlikely, but it is difficult to evaluate. There may also be some small discrepancies in the cell modeling which are compensated for in the primary absorbance correction by the curve fitting, but which are not symmetrical with respect to secondary absorbance and thus go uncorrected. Such asymmetric errors could include reflection of the excitation beam from the quartz light pipe, effects of the inlet and outlet ports of the cell, refractive index effects, and changes in the fiber optic transfer function which are a function of wavelength.

E. Conclusions

The fiber-optic coupled front surface fluorescence flow cell appears to function quite well for primary-absorption inner-filter effect corrections. It is low volume, tolerates vibrations and cell

movement, and is easily optically coupled to the excitation and emission monchromators. The transmittance monochromator could also be similarly coupled, making this cell ideal for a variety of flow methods. Since the primary absorbance and fluorescence can be simultaneously measured on the millisecond time scale, this instrument is readily adaptable to kinetic methods, including stopped-flow mixing systems. Reaction monitoring can be based on either absorbance or fluorescence alone, or absorbance information could be used to flag for inner-filter effect errors and to correct them. Alternatively, one species could be monitored by absorbance while another was simultaneously monitored by fluorescence.

A principle disadvantage of this instrument is the need for 3 light filters. Although these would ideally be matched monchromators, in certain dedicated applications bandpass filters could be used. This particular cell also has an appreciable problem with a high fluorescence blank signal which may be attributable to the innate fluorescence of cell materials or adsorbed materials, or a result of stray light from the back-scattered excitation beam. Poor wash characteristics are also apparent, which could be a result of adsorption or trapping in the cell. Future cells should probably not be constructed with the black Delrin used, since chemical degradation of the black Delrin has been observed in this lab. Graphite filled Teflon or white Teflon (a modified theory may be required) would perhaps be preferred.

With matched, stepper-motor driven monochromators, secondary-absorbance corrections could be automated. Stepper-motor coupling should improve the wavelength accuracy and setting

reproducibility, thereby improving correction accuracy. The excitation and emission monochromators could be programmed to repeatedly slew between excitation and emission wavelengths to determine the absorbance at both wavelengths for the same solution. In addition, a microcomputer controlled emission monochromator would permit corrected excitation and emission spectra to be measured.

The signal-to-noise ratio (SNR) characteristics of this instrument also appear to be better than those for the Christmann cell shift instrument. This is probably and predictably attributable to the elimination of the collimation requirement of the method of cell shift. As a comparison, the cell shift instrument of Christmann achieves a maximum absorbance SNR (signal/s.d.) of about 1000 at A = 1.5, (12) whereas this instrument achieves a SNR of about 5000 at A = 1.5. The use of both pre- and post-cell monochromators also provides excellent absorbance linearity and better immunity to reemission errors as occasionally observed in the absorbance measurements with the method of cell shift. For the maximum fluorescence signal observed with the cell shift instrument, 5 nA, the SNR was approximately 170. For this method a SNR of 900 is achieved under similar conditions. Similarly, for 20 μM QS excited at 365 nm on the Hg line of a 150 W Hg-Xe arc and observed at 436 nm with 4 nm bandpasses, the Christmann corrected fluorescence SNR was approximately 60. For this instrument under identical conditions except for 438 nm emission and excitation with a 150 W Xe arc the SNR exceeds 500, despite identical bandpasses but narrower slits and without the advantage of the higher Hg-Xe arc flux at 365 nm.

Two other practical problems, though surmountable, remain with the present instrument. First, Xenon arc intensity variations of 10% to 20% occur over the course of most experiments. Despite the use of a reference detector, such large drifts cannot be adequately corrected, causing inaccuracies in the data. An optical feedback stabilized arc could minimize both the short term variations and long term drift to less than 1.0%. Matching of the reference and transmittance detection circuits, in the same housing if photodiodes are used, would also likely reduce drift. Lastly, bifurcation of the end of the excitation fiber optic and randomization of these fibers would permit a more accurate and homogeneous sampling of the excitation beam by the reference detector. Currently, the reference and excitation beams are slightly different with respect to both sampling geometry and wavelength, and both of the photodiodes and their amplifying circuits are different. The other major problem in this instrument is 1/f noise. Thus far, this problem has been the overwhelming source of error, particularly at low light levels, where the dark current 1/f contribution becomes significant. Further useful studies of precision, SNR, reproducibility, linearity, and accuracy cannot be completed until this 1/f noise is vastly reduced. This problem could be eliminated by chopping the source beam. A simple mechanical chopper could easily be used in conjunction with the microcomputer at chopping rates between 100 and 500 Hz.

CHAPTER IV

INSTRUMENTATION AND SOFTWARE FOR LUMINESCENCE MEASUREMENTS

A. Introduction

The development of the research instrumentation used in the experiments outlined in this thesis required a system which incorporated intelligent data acquisition and parameter control. Because both flexibility and adaptability are desirable, a computer system is the obvious choice, allowing evolution of instrument hardware or applications to be accomodated by software. A computer system also facilitates accurate data storage, transfer, and retrieval, giving the chemist greater power to make decisions and draw conclusions through the use of graphic display and statistical evaluation.

B. A Hierarchical Computing System

A hierarchical computing sytem was used. This system links a low cost and flexible Intel 8085-based (56) microcomputer system with a more powerful LSI 11/23 (28) "mini"-computer. The 8085 microprocessor and its associated family of support chips form an efficient system which can be readily adapted to many laboratory applications. The interrupt structure of the 8085 system gives quick and efficient response to the needs of peripherals and interface. Serial communication beween the 8085 and the 11/23 gives the user the

advantages of custom interface design for data acquisition and control of the 8085 and the power of the 11/23 for editing, calculating, cross-assembly, compilation and mass storage. The 8085 also has greater portability or can be affordably dedicated to a single instrument. This computer networking system allows several microcomputer-based instruments to share the software and hardware facilities of the 11/23.

The chief drawback of the networked system is the lack of high-speed access to the 11/23 upon which the instrument is dependent. Because the serial communication is relatively slow, program downloading or data uploading and the requirements in writing the software to facilitate these transfers are time absorbing and often difficult. Total portability is also limited due both to the requirement of a serial link and the real or apparent dependence of the user on the powerful facilities of the 11/23 RSX-11M environment. However, local mass storage could overcome the physical dependence upon the 11/23.

C. A Modular Microcomputer

The 8085 microcomputer used for these (and other) instruments was a versatile system designed by Bruce Newcome within the research group of Dr. C. G. Enke (22). Its general design attributes include modularity and flexibility in adapting and expanding its peripherals. Various capabilities can be added to the computer via small boards of selected functionality. Individual functions can be easily upgraded as more powerful integrated circuits become available. Reliability

and compactness are enhanced through selection of large scale integrated circuits, wherever possible. The microcomputer's usefulness was further extended by constructing it within a single portable case, with standard BNC connectors for analog input and output (I/O) and a standard "D" type connector for parallel digital I/O. The instrument has available 4 parallel analog inputs, 2 parallel analog outputs, 22 programmable digital I/O lines, and 2 serial RS-232 links.

1. Basic Modules

The microcomputer hardware capability is comprised of the following modular subunits:

1. CPU - 8085A microprocessor and associated bus transceivers and buffers, status indicator LEDs, and hardware RESET switch.
2. ROM/RAM - Up to 32K of any combination of the designated 2K read only memory (ROM) or random access memory (RAM) chips. A total of 4K of ROM and 12K of RAM was used for the chemiluminescence experiments, while 10K of ROM and 14K of RAM was used for the fluorescence experiments.
3. Programmable Interrupt Controller - The PIC intelligently expands the processors interrupt capacity and capabilities.
4. Dual USART - Two RS-232 communications ports are available. One port is assigned to the user's terminal and the other is usually used for I/O with the 11/23.
5. Chip Select - The addressing of most devices other than the ROM/RAM and CPU boards is accomplished with the aid of this single

decoding module. Unnecessary redundancy of decoding circuits is thereby eliminated at a savings of time, space, and expense.

Four other specialized circuits were used to customize this basic microcomputer to realize its intended purposes. A dual-DAC board employing 2 8-bit digital-to-analog converters was added to provide triggered X-t or X-Y oscilloscope display of data or X-Y/X-t recorder plots. The three remaining circuits were designed by the author. Two of these circuits (timer and ADC) are currently being used in other microcomputers, while the third (S/H-MUX) is perhaps the most novel.

2. Counter/Timer II Board

The Counter/Timer II board supercedes an earlier board based on the Intel 8253-5 device with the Advanced Micro Devices 9513 System Timing Controller. This board is simple in external design, belying an extremely powerful microprocessor designed for counting, sequencing, and timing applications. To fully appreciate the usefulness, flexibility and complexity of this device, the reader is referred to more complete documentation (57). The 9513 contains five, 16-bit, individually programmable counters. Applications of interest include time-of-day clocking, real-time program independent clocking, count down/up, polled or interrupt timing for data collection sequencing or peripheral servicing, programmable waveform synthesis, and event count accumulation.

The interface of the 9513 to the microcomputer bus is straightforward. Bus lines D_{0-7} are interfaced to the 9513 I/O pins DB_{0-7} through the 74LS245 tri-state transceiver. NOT WRITE, NOT CHIP

SELECT, and NOT READ are interconnected between bus and 9513 (pins 9-11, respectively), and the NOT READ and NOT CHIP SELECT bus lines are also connected to 74LS245 lines SEND/NOT RECEIVE (pin 1) and NOT CHIP ENABLE (pin 19), respectively. Bus line A_0 is connected to 9513 input CONTROL/NOT DATA (pin 8). Ten kilohm pullup resistors are connected beween power and 9513 lines DB_{8-15} and $SOURCE_{1-5}$. An external crystal-controlled TTL-level output device is the preferred timing base for the 9513 since the internal oscillator was found to be unreliable. Such a device can be added to the board in the multi-purpose wire-wrap area provided.

3. Analog Input

The analog input section of the microcomputer is comprised of 4 sample-and-hold (S/H) inputs multiplexed into a 12-bit analog-to-digital converter (ADC). This circuit allows simultaneously gated sampling of up to 4 analog signals, followed by sequential analog-to-digital conversion of each signal sample. Analog sampling and multiplexing and the associated bus interface are located in a single module appropriately called the sample-and-hold multiplexer (S/H-MUX) board. The ADC and associated curcuits are on a separate card which is one of several modules that form the set of optional functions commonly available for other microcomputers of this type.

4. Sample-and-Hold Multiplexer Board

The S/H-MUX is described here as 3 sub-units: the differential input S/H, the multiplexer-S/H output, and the S/H gating and MUX channel addressing decoder, latch, and indicator circuit, as shown in Figures 4-1, 4-2, and 4-3.

(a) Differential Input Sample-and-Hold

Four identical differential input inverting S/H circuits form the first stage of the analog input circuit. The difference input (58) S/H, is based on a commonly available monolithic circuit S/H (Datel Intersil SHM-IC-1; Analog Devices AD583; Harris HA-2520/2425) (59-60) modified for improved differential input characteristics, as shown in Figure 4-1. RN60-type metal-film 100 kilohm resistors (R_1-R_4) were carefully matched to better than 0.02% using a portable bridge. This provides excellent common mode rejection (measured to be better than 85 dB), while providing immunity to ground loops between the analog input commons. An alternate differential input circuit considered would have required 4 instrumentation amplifiers at considerably higher cost and/or complexity. A 10,000 pF polystyrene capacitor was used to provide S/H characteristics consistent with the overall analog input design requirements: 12 microsecond acquisition time, 5 mV per second droop, 0.002% hold-mode feedthrough, 2 mV sample-to-hold offset error, and 0.005% sample-to-hold gain error. Each of the 4 S/Hs has an independent digital control permitting on-board (described later) or external mode control for flexible operation initiated by software or asynchronous events.

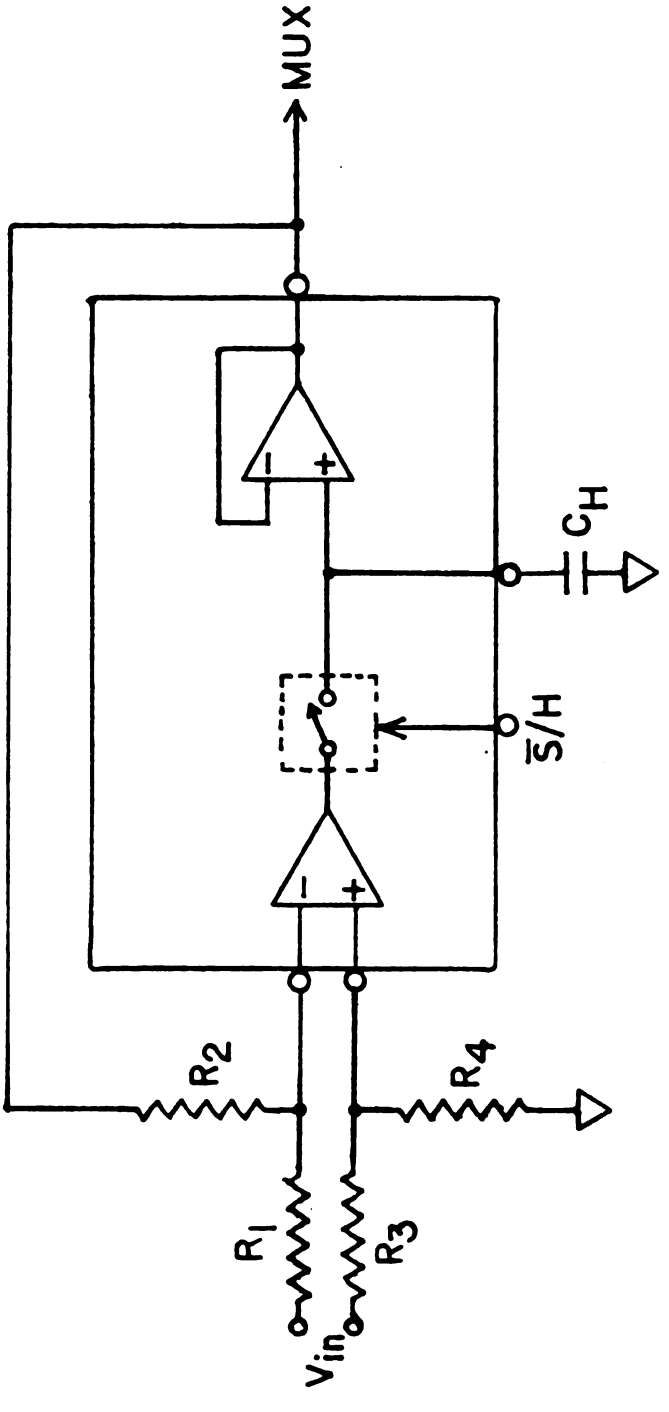

Figure 4-1. Differential input sample-and-hold.

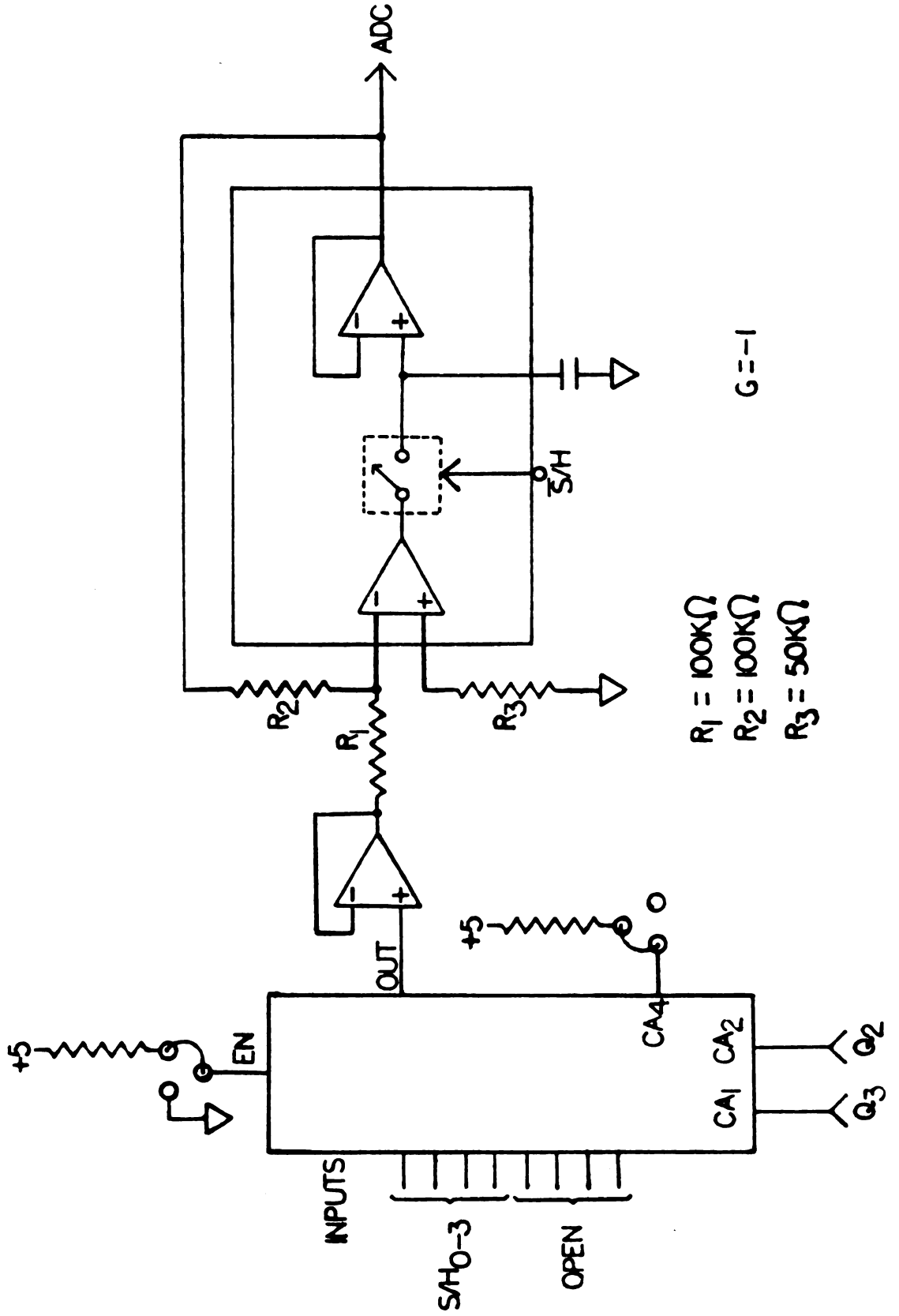

Figure 4-2. Multiplexer - S/H output.

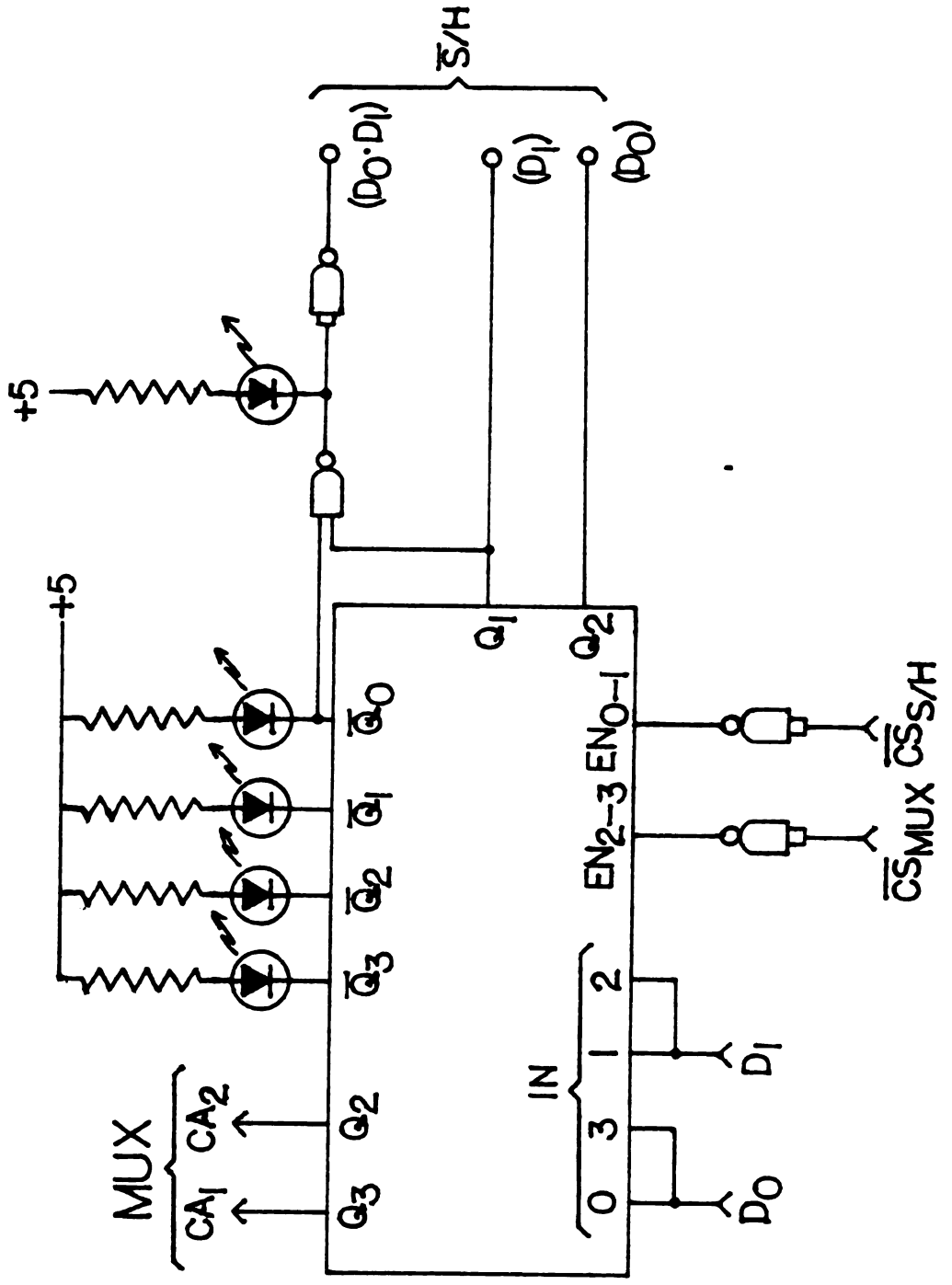

Figure 4-3. S/H gating and MUX channel address latch decoder and indicator.

(b) Multiplexer - S/H Output

All of the difference-input S/Hs are multiplexed by a CMOS 8-channel multiplexer (59). The MX-808 multiplexer was chosen because the inputs have overvoltage protection and break-before-make switching is used. This monolithic device is also popular and reasonably priced. Channel decoding is software programmable via a decoded latch (discussed later). The MUX output is buffered by a simple LF351 (61) follower circuit to maintain transfer accuracy despite the finite MUX load impedance. The buffered output of the MUX is directed into an inverting S/H used as the ADC input buffer as shown in Figure 4-2.

(c) S/H Gating and MUX Channel Address Latch Decoder and Indicator

A 74LS75 quadruple latch and a 74LS00, as shown in Figure 4-3, are the integrated circuits used to provide a variety of S/H gating and MUX channel selection modes. A chip select ($\overline{CS}_{MUX}$) pulse at the multiplexer enable inputs (EN_{2-3}) latches the status of bus data lines D_{0-1}, to provide MUX channel selection via Q_3 and Q_2, respectively. LED lamps tied to outputs $\overline{Q}_2$ and $\overline{Q}_3$ give the microcomputer operator visual indication/diagnostic of the analog channel(s) chosen. Similarly, a second chip select ($\overline{CS}_{S/H}$) pulse at enable inputs (EN_{0-1}) latches D_{0-1} at Q_{0-1}, respectively. Along with latched outputs Q_{0-1} reflecting data lines D_{0-1}, a latched value for $D_0 \cdot D_1$ is also available for gating S/Hs. These three outputs provide a variety of jumper-selectable S/H modes for simultaneous or asynchronous software-controlled sampling.

5. General Purpose 12-Bit ADC Board

The ADC board was designed to be a relatively low cost, general purpose, medium speed, 12-bit ADC interface. A basic functional schematic is shown in Figure 4-4. The circuit is based on the AD574 (60), a successive approximation 12-bit analog-to-digital converter with a 35 µs conversion time. The AD574 (IC1) has an internal voltage reference, internal clock, and provides for a 10 V or 20 V range unipolar or bipolar analog input. The choice between unipolar or bipolar operation is provided at building time by the proper selection of components and jumpers, as described below:

Unipolar (0 to 10 V or 0 to 20 V):

P1 = 100 ohm potentiometer

P2 = 100 ohm potentiometer

R1 = 100 kilohm resistor, J1 to J7

R2 = 100 ohm resistor, J8 to J9

Jump J1 to J2

Bipolar (-5 to +5 V or -10 to +10 V):

P1 = 100 ohm potentiometer

P2 = 100 ohm potentiometer

Jump J2 to J3

Jump J4 to J5

Jump J5 to J7

Space is also provided for a S/H amplifier to be used as a non-inverting gain-of-one input buffer.

The digital interface is completed by a 74LS245 octal tri-state buffer (IC2), and a 74LS368 or 8T98 tri-state hex inverter (IC3). The

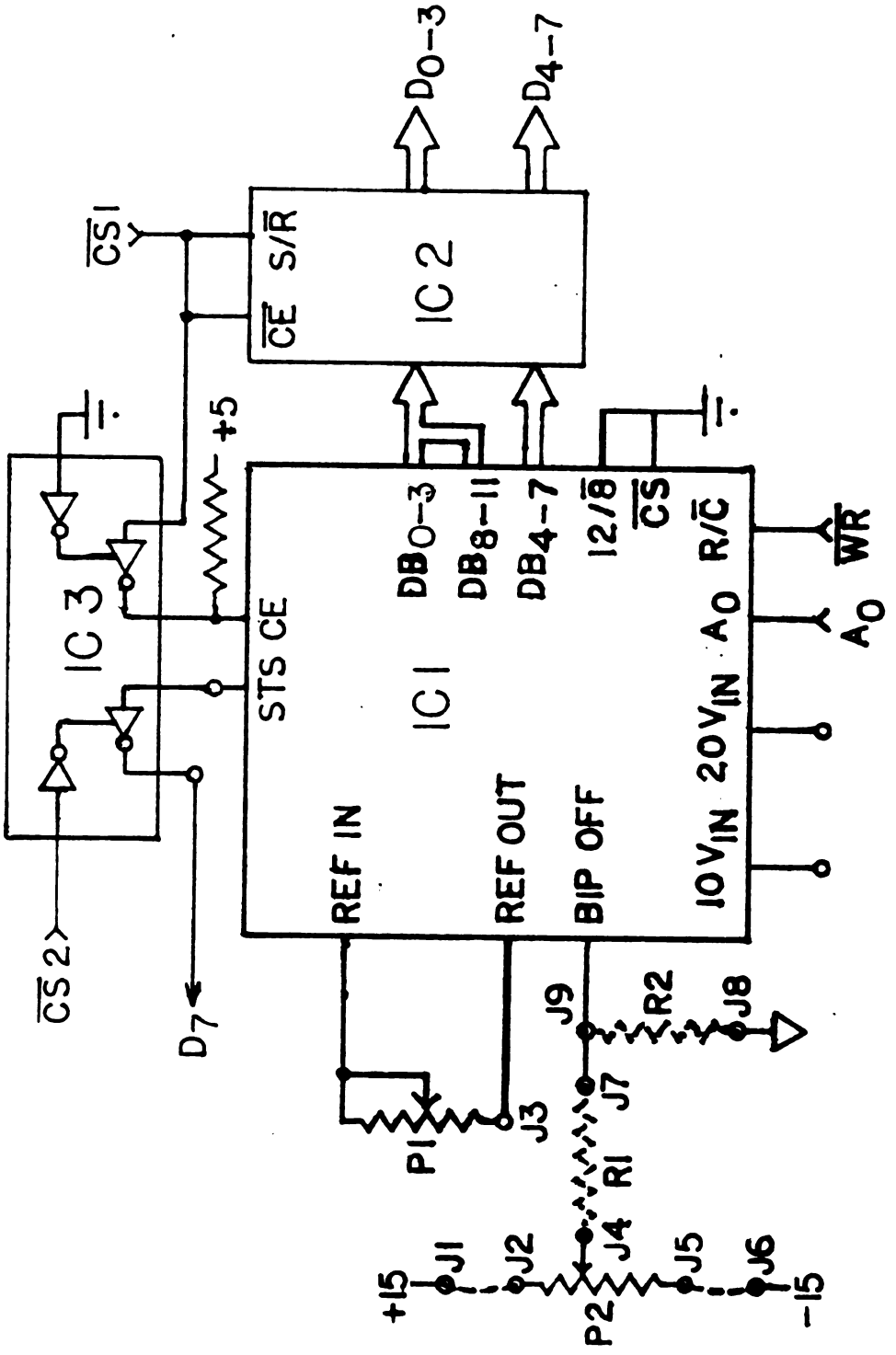

Figure 4-4. General purpose 12-bit ADC board.

octal buffer drives the ADC output onto the bus under the direction of $\overline{CS1}$. When reading, A_0 LO forces data bits DB_{4-11} (MSBs) onto the data bus, D_{0-7}. With A_0 HI, DB_{0-3} are forced onto D_{0-3}, and a binary 0000 is forced onto D_{4-7}. The conversion cycle is initiated by writing to the memory area of $\overline{CS1}$. During conversion, the status output line, STS, goes HI, until the conversion cycle is completed. This line is polled by the microprocessor by reading from the memory space of $\overline{CS2}$, where D_7 LO indicates that the ADC is busy. The STS line may also be used to asynchronously interrupt the processor at the end of the cycle and/or to trigger the S/H buffer to hold the analog input steady during the conversion cycle.

The first version of this board is still being used in the microcomputer described in this thesis. This board was originally found to be missing codes in the two or three least significant bits. This problem disappears when the bus is halted during the conversion cycle (the STS line is used to generate a microprocessor "wake-up" interrupt), indicating that the missing codes may be symptomatic of an undersized ground plane shielding the ADC from electromagnetic interference generated on the bus. This practice is still being used for this board; however, the ground plane has since been expanded on later boards. Additionally, an area has been added for an optional ±15 V dual-tracking voltage regulator, for those microcomputers whose busses do not already meet this need.

D. A Photodiode Detector

Three light detectors were used for the fluorescence experiments: a PMT for fluorescence detection, a photodiode detector for an excitation intensity reference and a photodiode for excitation transmittance detection. Photodiodes were used because of their durability and immunity to vibration, because they are not adversely affected by a very high photon flux, and because they are inexpensive, have a wide dynamic range, and are stable and devoid of hysterisis or memory effects. Additionally, they do not require a high voltage power supply. They can be easily integrated into a small package with the required power supply and current-to-voltage converter and amplifier. The reference photodiode detector was designed by Patton (54). A functional diagram of the device designed by the author is shown in Figure 4-5. A Hamamatsu S780-5BQ silicon photocell (62) develops a current which is converted to a negative voltage by the first op-amp. The feedback amplifier is switch selectable with the feedback resistance ranging from 100 KΩ to 1000 MΩ. The feedback capacitors were adjusted to maintain a 10 μs time constant. The second stage amplifier is a voltage follower with gain variable from 1 to 20. The third op-amp is an inverting, active filter with switch-selectable capacitors ranging from 100 pF to 10 μF for rise times from 10 μs to 1 s. All of the op-amps are LF351s. Power is internally supplied by an LM326 ±12 V dual-tracking voltage regulator. The regulator is in turn supplied by an external ±15 V supply via a shielded-twisted pair. Since very little noise is introduced into the metal enclosure (case common) by the power cord, and a very stable

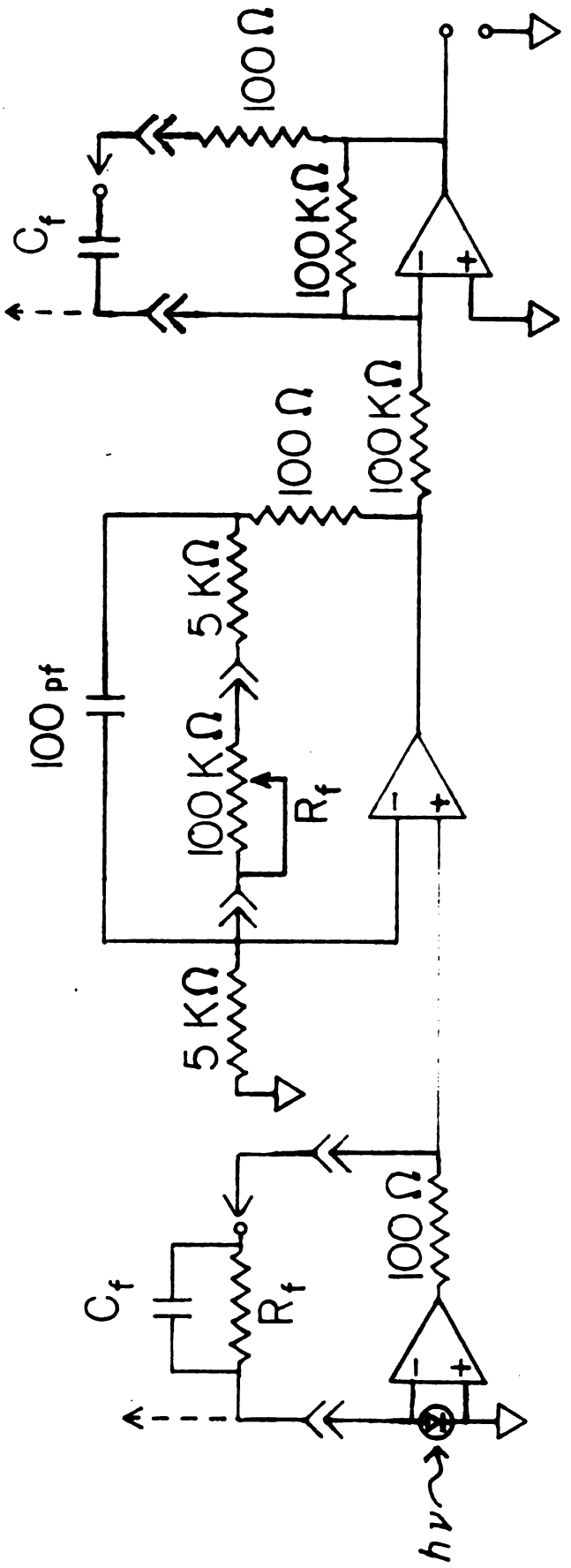

Figure 4-5. A photodiode detector.

power supply is maintained by the dual-tracking regulator, the detector circuit maintains a high quality, low drift output.

Unfortunately, silicon detectors have a very low quantum efficiency in the UV. Due to this inefficiency, higher gains are required, resulting in correspondingly greater amplifier noise and drift problems. This problem may well be reduced if the LF351 general-purpose op-amps were replaced with op-amps that had lower noise and drift characteristics. Alternatively, if studies below 370 nm continue, these detectors could be replaced by photomultiplier tubes which have much better quantum efficiencies in the UV. Lastly, users of photodiodes should be aware that the high IR quantum efficiencies may require an IR blocking filter to be used in conjunction with broadband cutoff, bandpass, or dichroic interference filters, as these filters often pass some IR wavelengths.

E. Microcomputer Software

1. Choosing a Microcomputer Language/Operating System

The choice of programing language used with this microcomputerized instrumentation was based on several factors. The decision must be made within the context of the experimental and hardware requirements, costs, ease of installation, availability, and strengths and weaknesses of a given language. A major requirement for the language of choice is that it permit maximum use of all the power and speed of the microcomputer while minimizing the difficulty of programming at both high and low levels. It should be relatively easy to learn and facilities for self-tutorial or other instructional

opportunity should be available. Documentation should be both broad in scope for the novice, and specific, accurate, and thorough for the expert. The language should facilitate computing at both the machine language or assembly level as well at a high level. At the low level, the programmer should be able to use all possible processor instruction codes to implement any task required for a given set of hardware. This code should also be easily merged with other high level programming. System constants and variables should be mutually accessible at both levels. High level programming should facilitate "housekeeping" of memory management for arrays, variables, constants, pointers and vectors. High level commands should be available for comparisons, jumps, loops, returns, and conditionals. Terminal and mass storage I/O tasks should be readily implemented. Ideally, the language might have a continuum of commands to cover programming from very low to very high levels. A facility for efficient and rapid high level mathematics should be included. (Although this usually takes the form of a floating point math package, fixed point math packages, as discussed later, are also viable options). The ideal microcomputer operating system environment would also provide facile editing, and rapid compilation and assembly. Error messages and program development techniques should reduce debugging time and frustration to a minimum. System firmware and user programs should be compact. Multitasking performance is an often desired option, while multiuser capability is of little probable value for a hierarchial environment. A file-structured system orientation is highly desirable. Ultimate power and flexibility in software with currently popular conventional languages (such as BASIC) often implies the maximum in development

time, maintainence time, expense, complexity, memory and execution time. Other options are worth considering.

2. SLOPS

Two languages were used for the experiments described within this thesis. The chemiluminescence experiments were conducted with the language SLOPS, written by Hugh Gregg. SLOPS is a minimum system which contains a kernel linking several very basic subroutines and providing for communications between the 8085 microcomputer and the 11/23 minicomputer host. Programs were written in 8085 assembly language mnemonics on the 11/23 and then cross-assembled and down loaded into 8085 memory for execution. This system has the advantages of using the powerful text editors and file-structure of the 11/23, but suffers from lengthy cross-assembly and serial communications times. High level computing was virtually unavailable on the microcomputer.

3. FORTH

FORTH, a rising star in microcomputer control systems languages, was used for the fluorescence instrument. FORTH is a readily exstensible language and features total system capability. Editing, compiling, assembly, math packages, and I/O are all available in compact firmware. A unique feature of FORTH is that it does not actually compile, but rather links programs or subroutines into new programs or subroutines. Programmers begin with a subset of useful subroutines called "words" in FORTH lingo. Programming entails

creating new words by linking previously defined words or assembly language commands. FORTH links/compiles quickly and is compact. Near ultimate speed is available only through linear programing in assembly language which obviates many of the advantages of FORTH. Since FORTH programs are ultimately a collection of highly nested subroutines, considerable time is spent by the FORTH executive in jumps and returns. For high level mathematics calculations, however, FORTH excels in speed because of its use of fixed point rather than floating point math, as has been convincingly argued elsewhere (63). Other criticisms of FORTH are its lack of a file structure, difficulties in documenting or reading FORTH programing , and the need for uniqueness of "word" naming. Multitasking and multiuser capability are also features which are potentially useful though not required.

F. Software for a Dual-Pathlength CL Spectrometer

All of the chemiluminescence experiments were run within the SLOPS microcomputer operating system/language. Programs were downloaded from the 11/23 via the serial link using a protocol in which the 8085 requested that the 11/23 download an object file and the 11/23 responded by downloading the file preceded by starting address and length. Since the 8085 response time was quicker than the transfer rate determined by the baud rate of 2400, no complicated handshaking was required.

The voltage from the current amplifier was sampled by a sample-and-hold amplifier and converted to digital form by the ADC. Signal integration over integral multiples of 16.67 ms (1 period of a

60 Hz signal) was employed to eliminate a significant 60 Hz noise component of the signal; a result of the very high gain characteristics of the instrument. For both cell sides, at each oscillation, 1006 A/D conversions were acquired by an interrupt-driven subroutine at 116 μs intervals, as determined by the Counter/Timer II board. These data were accumulated and rounded-off to form a 16-bit sum representing the signal integrated over seven 60 Hz periods (116.7 ms). At 2 samples per oscillation and 2 oscillations per second, this sampling rate resulted in an overall duty cycle of 47% for data collection. After subtraction of the dark current value, determined in a similar way just before each run, the signal values were stored in memory for later processing.

Data were stored as successive intensity pairs from alternate sides of the cell. After each run, data were uploaded to the 11/23 into a binary file. A more complicated protocol requiring a "receipt acknowledged" character from the 11/23 to the 8085 was required to allow for the slower 11/23 response time. Data were post-processed on the 11/23. Individual ratios were calculated for each intensity pair. Ten pairs were averaged and standard deviations for each mean were calculated. A weighted average was then calculated using all means. The integrated light intensity was similarly calculated by using the intensities from the long pathlength side of the cell. Using these ratio and intensity values, the absorbance, correction factor, and corrected intensities were all calculated and reported in tabular form.

G. Software for an Absorbance-Corrected Fluorimeter

The FORTH operating system is used for all of the fluorometry experiments. The 11/23 is used to transfer ASCII "blocks" into RAM buffers for subsequent linking into FORTH code. Such transfers are implemented on the 11/23 by FPIP (64). In conjunction with vectored routines in the microcomputer firmware, FPIP allows the 11/23 to appear to be a disk mass-storage device. Transfer protocols are similar to those with SLOPS, except that checksums are monitored to assure accurate serial transfer.

The voltage outputs from the three light detector circuits are simultaneously sampled at 5 ms intervals. Average signal values are accumulated from 2000 samples. Three FORTH words are used to conduct the fluorescence experiments. "DARKGET" obtains and stores the dark current values from the reference and transmittance detectors with the source blocked. With the source unblocked, "0GET" obtains a reference value from the reference detector, a 100% T value from the transmittance detector, and a blank background level from the fluorescence detector. "SPIN" executes an infinite loop which obtains current light values from the detectors in 10 s intervals and then calculates and displays the data in tabular form. The table contains the dark, reference, and light levels, the light levels corrected for dark current or background, the ratio of the current to the initial reference levels, the transmittance and reference-corrected transmittance, and the fluorescence and reference-corrected fluorescence. This tabular display format allows the user to examine the data in real-time, assessing drift and precision, as well as the

experimental trends. Currently, data are manually recorded from these tables for subsequent calculation of the absorbance, correction factor, and corrected fluorescence using a programmable calculator.

CHAPTER V

A UNIFIED MATHEMATICAL LUMINESCENCE VOLUME-SOURCE MODEL

A. Posing the Problem

A basic premise of the techniques presented in this thesis, as well as other absorbance-corrected luminescence techniques, is that the attenuation of the emission signal is a predictable phenomenon governed by geometry and Beer's law. Beer's law is simple, familiar, and easily applied. However, all to often, correction schemes have incorporated a falsely simplistic approach to the geometric aspects of the problem, or do not have clearly stated underlying presuppositions or supporting proofs. This chapter is an attempt to provide a partial proof or test of some of the geometrical assumptions applied in the absorbance-corrected techniques of Chapters II and III. This work may also prove useful in extending or modifying these techniques in new ways, or for comparison to other approaches at geometrical descriptions.

A luminescence signal represents the integrated intensity from many planes of emitters, each affected by attenuation of light as a function of its respective depth according to Beer's law. A primary difficulty in modeling Beer's law attenuation arises from an additional geometry complication. Each of these planes has a particular optical efficiency with which it is excited or observed, and even at different locations on the plane, this efficiency function

may vary significantly. Since modeling the luminescence signal requires mathematical integration over all of the emitting volume, an accurate model of luminescence as a function of absorbance cannot be obtained without careful consideration of the geometry of the excitation and emission light paths. A mathematical model is presented here that considers the excitation and emission geometry at any point in the active volume of interest. Integration of this point-source model over the entire planar area of emission produces an expression that can be used to evaluate changes in excitation and emission cross-section as a function of depth, independent of changes which are a function of Beer's law attenuation.

In the absorbance-corrected chemiluminescence technique described in Chapter II, an underlying assumption implicit in Equation 2-2 is that the cross-section of detected light is constant with increasing depth (independent of absorbance attenuation). Experimentally, this restriction was approximated by using a collimator. This collimation approximation permits simplified expressions to be used for the derivation and correction of the inner-filter effect. Later in this chapter, this experimental configuration is tested to validate its effectiveness by a comparison at various depths of emission cross-sections determined by this model.

For the fiber-optic front-surface fluorescence cell, the point-source, excitation/emission model is linearly combined with the fiber-optic angular acceptance function (AAF), which describes the decrease in transmittance of the fiber-optic with a decrease in the incidence angle measured with respect to the fiber axis (65). For UV fiber-optics, the AAF is nearly Gaussian in distribution, typically

having a half-width of 20° to 30° at half-height (66). The sine of the angle at which the light input or output falls to 50% of its maximum is refered to as the numerical aperture (NA) and is a measure of the light-gathering power of the fiber optic. The NA decreases with decreasing fiber length and decreasing wavelength of light. Since the length of the fiber-optic does not change, and the wavelength range is limited, the effects of figer length and wavelength may be neglected here. The AAF is integrated with the point source model over all angles of emission, and all point sources are integrated over each plane of emission normal to the cell axis, to determine the transfer function referred to in Chapter III.

B. The Model

For a point source emitting light into 4π steradians (all directions) with equal intensity, the fraction of light which passes through a hole in a plane of given dimensions, orientation and distance from that point source can be calculated.

Assume that the point source is at the origin (0,0,0) (see Figure 5-1), and that the hole is described by a circle centered at:

$$z = d$$

$$y = 0$$

$$x = r$$

with a radius of R.

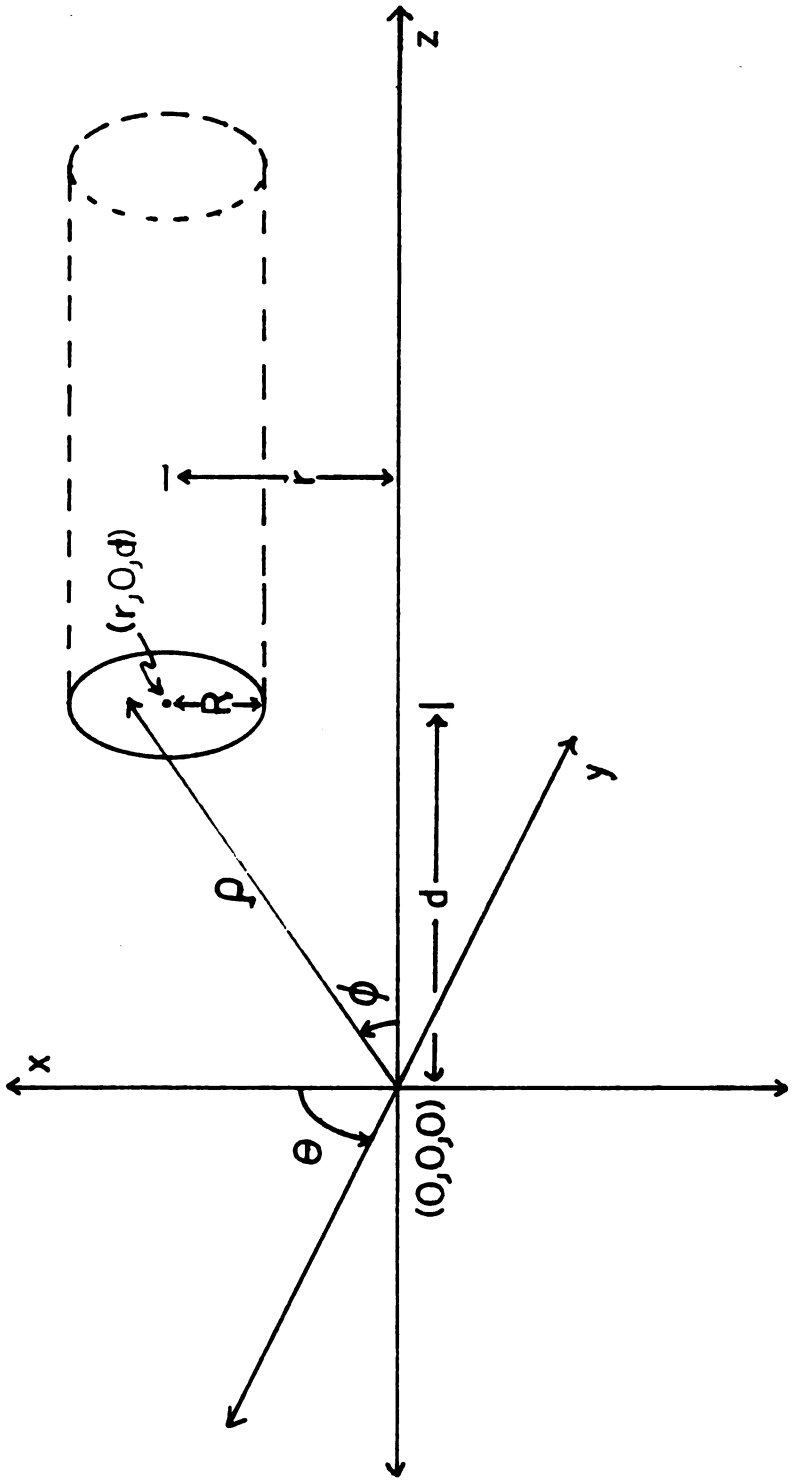

Figure 5-1. Geometrical model of point-source.

The equations of this circle are (Cartesian coordinates):

$$z = d \tag{5-1}$$

$$(x - r)^2 + y^2 = R^2 \tag{5-2}$$

To transform to spherical coordinates:

$$x = \rho\sin(\phi)\cos(\theta)$$

$$y = \rho\sin(\phi)\sin(\theta)$$

$$z = \rho\cos(\phi)$$

$$\phi = \arccos(z/\rho)$$

$$\theta = \arctan(y/x)$$

Transforming Equation 5-1 into spherical coordinates:

$$\rho\cos(\phi) = d \tag{5-3}$$

Transforming Equation 5-2 into spherical coordinates:

$$\rho^2\sin^2(\phi) - 2\rho r\sin(\phi)\cos(\theta) = R^2 - r^2 \tag{5-4}$$

The fraction of light through this circle is given by the solid angle formed between the point source and the circle, divided by 4π steradians. The element of solid angle is

$$d\omega = \sin(\phi)\, d\theta d\phi \tag{5-5}$$

Thus, the solid angle is obtained by integrating over the limits of ϕ and θ:

$$\omega = \int_{\phi} \int_{\theta} \sin(\phi)\, d\theta d\phi \tag{5-6}$$

There are two cases for integration:

i. For $r \leq R$

ϕ extends from 0 to $\arctan((R - r)/d)$ where

$\theta = 2\pi$

ii. for $r > R$

ϕ extends from $\arctan((r - R)/d)$ to $\arctan((r + R)/d)$

Equation 5-4 is then solved for θ using Equation 5-3:

$$\theta = \pm\arccos(c) \tag{5-7}$$

where

$$c = (d^2\tan^2(\phi) - R^2 + r^2)/(2dr\tan(\phi)) \tag{5-8}$$

Putting the limits of integration into Equation 5-6 for cases i and ii:

$$\omega = \int_0^{\alpha}\int_0^{2\pi} \sin(\phi)\, d\theta d\phi \quad + \quad \int_{\gamma}^{\beta}\int_{-\arccos(c)}^{+\arccos(c)} \sin(\phi)\, d\theta d\phi \tag{5-9}$$

where

$\alpha = \arctan((R - r)/d))$

$\beta = \arctan((R + r)/d))$

$\gamma = \arctan((r - R)/d))$

and c is given by Equation 5-8.

Equation 5-9 simplifies to

$$\omega = 2\pi\left[1 - d/(d^2 + (r - R)^2)^{1/2}\right] + 2\int_{\arctan((r - R)/d)}^{\arctan((R + r)/d)} \sin(\phi)\arccos(c)\, d\phi \qquad (5\text{-}10)$$

Equation 5-10 can be numerically integrated using Simpson's rule. The fraction of light is then

$$\text{fraction} = \omega/4\pi \qquad (5\text{-}11)$$

C. Application to CL Techique

To determine the fraction of light which is emitted from a point through a cylindrical collimator, Equation 5-10 is numerically integrated using the circle defined by the collimator exit to determine the values of R, r, and d for the limits on the first part of the equation. For the second part of Equation 5-10 the low ϕ limit for $r \geq R$ is defined by the collimator entrance; for $r \leq R$ the low ϕ limit is always defined by the collimator exit. The large ϕ limit is determined by the collimator exit. These limits are apparent from the geometry (Note: The use of a long cylinder such as the leftover cardboard tube from a roll of paper towels is useful for visualizing this problem). Arcos(c) is the smaller of the values taken for both the exit and entrance. (This yields the limiting value.)

The fraction of light from a plane can be calculated by numerical integration of Equation 5-11 over all points of the active plane, and is analogous to the integration of the area of a circle:

$$\text{cross-section} = \int_0^{r_c} \text{fraction}(d) \cdot r_c \, dr_c \qquad (5\text{-}12)$$

where r_c is the radius of the cross-sectional area, and is defined by the intersection with the plane of interest of a ray intersecting the collimator axis and both circles formed by the ends of the collimator (see Figure 5-1).

Equation 5-11 was numerically integrated using Simpson's rule with the FORTRAN program POINT on a PDP LSI 11/23. To reduce potential roundoff errors, all calculations, constants, and variables were double-precision. POINT was compared to the program CALLOBS which uses a completely different approach employing elliptical integrals. CALLOBS is based on an independent derivation by Dr. Gale Harris (67). Both programs produce self-consistent results for a variety of combinations of the variables d, r, and R. POINT was then used as a subroutine to numerically integrate Equation 5-12 in the program SLICE. Results of SLICE have shown that the relative change in the amount of light observed from each plane from the front to the back of the chemiluminescence cell is approximately +4%, agreeing with experimental evaluations within experimental error. The effect of this increasing cross-section of detected light with increasing depth was discussed in Chapter II, and it appears to be a negligible effect. This validates the collimation assumption used in the derivation of the correction method.

D. Application to the Fiber-Optic Coupled Fluorescence Technique

To determine the transfer function, T(x), discussed in Chapter III, the fiber-optic angular acceptance function (AAF) is linearly

combined with Equation 5-9 before integration over ϕ. The AAF was evaluated by measuring the relative optical output of the fiber-optic as a function of the angle of incidence of a collimated light beam as described by Math (68). The data were found to fit the empirical equation

$$AAF(\phi) = e^{-(\phi/0.35)^{1.6}} \qquad (5\text{-}13)$$

where ϕ is given in radians. Equation 5-13 was linearly combined with Equation 5-9 which in turn was integrated over all angles and points as with Equations 5-11 and 5-12, resulting in several excitation/emission cross-sections determined for various depths. Results show that the fiber-optic cell excitation/emission cross-section decreases exponentially with increasing distance from the fiber-optic into the cell. This model was used to derive a somewhat empirical transfer function based on this prediction of an exponentical decay, as discussed in Chapter III. The resultant transfer function based on this model is combined with theoretical fluorescence equations to derive a mathematical correction factor which accurately calculates absorbance-corrected fluorescence.

CHAPTER VI

CONCLUSIONS

A dual-pathlength method for absorbance-corrected chemiluminescence has been demonstrated. Experiments have shown that correction is possible to greater than 0.75 absorbance units. Extension of the correction procedure to higher absorbance values is predicted if the collimator artifacts are eliminated, the SNR improved, and the emission bandwidth narrowed.

Further studies should be initially directed toward increasing SNRs. This should be possible through increased light collection efficiency by reducing or eliminating the collimation requirement and extending the theory to account for these changes. The theory might be extended through the use of luminescence volume-source models, such as the model presented in Chapter V. Fiber optic coupling could be used for light collection from a cylindrical cell similar to the fluorescence cell described in Chapter III. Pathlength could be adjusted by means of a piston alternately moving toward and away from the fiber-optic, or conversely by moving the fiber-optic as a piston within the cylinder. Curve-fitting of pathlength vs. signal intensity information for a solution where A = 0.00 could be used to develop an accurate light collection transfer function to convolute with the function describing Beer's law attenuation.

Other obvious improvements could include the incorporation of photon-counting detection and/or chopping of the light signal to reduce 1/f noise. A thermo-electrically cooled PMT housing would increase the reliability and convenience of cooling. Additionally, since the sensitivity of the PMT is a function of temperature, a more reliably thermostatted housing should reduce temperature induced drift errors.

A multichannel detector such as an intensified diode array would be useful for multiple wavelength studies. Simultaneous correction at all wavelengths is possible, provided that the SNR is sufficient at each wavelength. With improved instrumentation and SNR, further theoretical and chemical investigations could be pursued. Absorbance-corrected chemiluminescence with a narrow wavelength bandpass should be tested at high absorbance values to see if currently observed deviations are stray-light induced due to nonmonochromaticity, as was suggested.

With the development of methods for faster measurements many other chemiluminescent reaction systems could be studied. For example, the rapid hypochlorite-luminol reaction might have the advantage of negligible background absorbance. Applications in clinical chemistry could be investigated, where inner-filter effects have been noted for such interferents as riboflavin and erythrocyte contamination, as mentioned in Chapter III.

Finally, a most valuable but equally or more difficult problem to deal with is reemission. Since most chemiluminescence systems do exhibit reemission, a correction method which permits or accounts for reemission would be very valuable.

An absorbance-corrected fluorescence method for a flow cell has also been demonstrated. The primary absorbance correction has been demonstrated to be accurate to within 1% to an absorbance of 3.0. Secondary-absorbance correction to an absorbance of 3.0 is accurate, with all errors below 10%; however, this figure might easily be reduced with improvements in technique brought about by monochromator automation, as discussed in Chapter IV.

A variety of other possible instrumental improvements have already been discussed in Chapter III, particularly methods for reducing 1/f noise, such as source stabilization and chopping. Reduction of 1/f noise and the fluorescence background signal would also extend the fluorescence detection limit, a figure which cannot now be reasonably estimated because of 1/f noise.

As discussed earlier, photon-counting, photomultiplier cooling, or intensified array fluorescence detection might prove useful. Alternate methods of secondary-absorbance correction, such as the moving piston method for chemiluminescence as suggested above, might permit primary and secondary absorbance corrections in near real-time. Another option might be to replace the quartz light pipe with another bifurcated fiber-optic, which could be used for simultaneous transmittance and 180° fluorescence detection. The 0° and 180° fluorescence signals will vary in significantly different ways as a function of secondary absorbance. With proper modeling and curve fitting, a secondary-absorbance function could likely be derived based on the ratio of 0° and 180° fluorescence. Such a cell could be used for primary- and secondary-absorbance corrected fluorescence on the millisecond time scale.

Excitation efficiency could also be improved by replacing the current crude lamp and lens assembly with a collimated Eimac lamp and achromatic beam condenser to direct a more intense, narrow beam into the excitation monochromator. Computer-controlled slit programming of all monochromators could be used to optimize the slit width for varying absorbance conditions - narrow at high absorbance, wide at low absorbance.

Software development of the current instrument could also be done to provide total calculation capabilities of absorbance values and correction factors, as well as collection and transfer of data files to the 11/23 for hardcopy or graphic output.

As with chemiluminescence, reemission errors are a dominating limitation of absorbance-corrected luminescence methods. Development of instrumentation which could correlate concentration and luminescence signal, despite inner-filter or reemission effects, would expand the number of applications of luminescence techniques immensely. With the absorbance-corrected fluorescence flow cell, an exponential dilution technique might prove useful for diagnosing or evaluating reemission effects by comparison of the dilution vs corrected fluorescence curves of negligible reemission solutions, to the curves of solutions which are suspected of having reemission.

Unfortunately, this fluorescence system has not been sufficiently developed nor has time allowed for an investigation of several analytical applicaitons of interest. This instrument is ideally suited for kinetic, low volume, primary absorbance-corrected fluorescence methods. Applications in clinical chemistry are of interest, since several homogenous assays of blood plasma suffer from

high primary absorbance (69). As an example, many Homogenous Enzyme Multiplied Immunoassay Technique (EMIT) (70,71) methods determine NADH by its rate of formation in the presence of blood plasma. Since absorbance detection is used, longer reaction times are required than might be required for an absorbance-corrected fluorescence technique. Fluorescence Immunoassay Analysis (FIA) (69) has similarly become popular in clinical laboratories, but occasionally suffers inner-filter effect errors. Other clinical methods could also benefit from absorbance-corrected fluorescence instrumentation (72,73).

BIBLIOGRAPHY

BIBLIOGRAPHY

(1) Beijerink M. W. Arch. Neerl. Sci. 1889 23, 416-427.

(2) Rauhut, M. M. Kirk-Othmer Encycl. Chem. Technol., 3rd Ed. 1979 5, 416-450, M. Grayson and D. Echroth (Eds.). Wiley, New York.

(3) Seitz, W. R.; Neary, M. P. Anal. Chem. 1974 46, 188A-202A.

(4) Cormier, M. J.; Hercules, D. M. ; Lee, J., Eds., "Chemiluminescence and Bioluminescence," Plenum Press, New York, N. Y., 1973.

(5) Kricka, Larry J.; Carter, Timothy J. N., Eds., "Clinical and Biochemical Luminescence", Clinical and Biochemical Analysis, Vol. 12, Dekker, New York, 1982.

(6) Seitz, W. R.; Neary, M. P. Methods Biochem. Anal. 1976 23, 161-188.

(7) Whitehead, Thomas P.; Kricka, Larry J.; Carter, Timothy J. N.; Thorpe, Gary H. G. Clin. Chem. 1979 25, 1531-1546.

(8) Wampler, John E.; Mulkerrin, Michael G.; Rich, S. Edwin, Jr. Clin. Chem. 1979 25, 1628-1634.

(9) Van Dyke, Knox; Van Dyke, Cynthia; Udeinya, Joseph; Brister, Calvin; Wilson, Mark Clin. Chem. 1979 25, 1655-1661.

(10) Marino, D. F.; Ingle, J. D., Jr. Analytica Clinica Acta 1981 124, 23-30.

(11) Christmann, D. R.; Crouch, S. R.; Holland, J. F.;Timnick, A. Anal. Chem. 1980 52, 291-295.

(12) Christmann, D. R.; Ph.D. Thesis, Michigan State University, East Lansing, MI, 1980.

(13) Christmann, D. R.; Crouch, S. R.; Timnick, A. Anal. Chem. 1981 53, 276-280.

(14) Stieg, Scott; Nieman, Timothy A. Anal. Chem. 1978 50, 401-404.

(15) Abbott, Edwin A. "Flatland", Dover, New York, 1952.

(16) Cadillac Plastics and Chemical Co., Flint, MI.

(17) Silicon Rubber Sealant, Dow Corning Corporation, Midland, MI.

(18) Model EU-721-11, GCA McPherson, Acton, MA.

(19) Model H-10, Instruments SA, Metuchen, NJ.

(20) Hoyt, S. D.; Ingle, J. D. Anal. Chem. 1976 48, 232-234.

(21) Model 427, Keithley Instruments, Cleveland, OH.

(22) Newcome, Bruce; Enke, C. G. , Michigan State University, private communication.

(23) Fisher Scientific Compay, Fairlawn, NJ.

(24) Aldrich Chemical Company, Milwaukee, WI.

(25) Mallinckrodt, St. Louis, MO.

(26) Matheson Coleman and Bell, Norwood, OH.

(27) G. Frederick Smith Chemical Co., Columbus, OH.

(28) LSI 11/23, Digital Equipment Corp., Maynard, MA.

(29) Lee, John; Seliger, H. H. Photochem. Photobiol. 1970 11, 247-258.

(30) Pilipenko, A. T.; Barovski, V. A.; Kalininchenko, J. E. Zh. Anal. Khim. 1978 33, 1880-1884.

(31) Burdo, T. G.; Seitz, W. R. Anal. Chem. 1975, 47, 1639-1643.

(32) MacDonald, A. ; Chan, K. W. ; Nieman, T. A. Anal Chem. 1979, 51, 2077-2082.

(33) Chang, C. A.; Patterson, H. A. Anal. Chem. 1980 52, 653-656.

(34) Rauhut, M. M. Acc. Chem. Res. 1969 2, 80.

(35) Scott, G.; Seitz, W. R. Analytica Chim. Acta 1980 115, 221-228.

(36) Dye, J. L.; Nicely, V. A. J. Chem. Ed. 1971 48, 443-448.

(37) Dye, J. L.; Nicely, V. A.; Tehan, F.; Cochran, R.; Leckey, J., "KINFIT4 - A General Non-Linear Curvefitting Program", 1977, Chemistry Department, Michigan State University, E. Lansing, MI.

(38) Bullock, D. G.; Bunce, R. A.; Carter, T. J. N. Anal. Lett. 1979 12, 841-854.

(39) Guilbault, G. G. "Practical Fluorescence, Theory, Methods, and Techniques," Dekker, New York, 1973.

(40) Mitchell, Douglas G.; Garden, J. S. ; Aldous, K. M. Anal. Chem. 1976 48, 2275-2277.

(41) Tiffany; T. O.; Burtis, C. A.; Mailen, J. C.; Thackery, L. H. Anal. Chem. 1973 45, 1716-1723.

(42) Chen, R. F.; Hayes, J. E. Anal. Biochem. 1965 13, 523-529.

(43) Wirth, M. J.; Lytle, F. E. Anal. Chem. 1977 49, 2054-2057.

(44) Adamsons, Karlis, M.S. Thesis, Michigan State University, East Lansing, MI, 1982.

(45) Adamsons, Karlis; Timnick, Andrew; Holland, John F.; Sell, John E. Anal. Chem. 1982 54, 2186-2190.

(46) Lloyd, J. B. F. Analyst 1980 105, 97-109.

(47) van Slageren, R.; den Boef, G.; van der Linden, W. E. Talanta 1973 20, 501-512.

(48) Smith, R. M.; Jackson, K. W.; Aldous, K. M. Anal. Chem. 1977 49, 2051-2053.

(49) Tietz, Norbert W., Ed. "Fundamentals of Clinical Chemistry," Saunders, Philadelphia, PA, 1976.

(50) Maxlight Optical Waveguides, Inc., Phoenix, Arizona.

(51) Wilmad Glass Co., Inc., Buena, NJ.

(52) Model 91087, Farrand Optical Co., Inc., Valhalla, NY.

(53) Model CA-150, Illumination Industries, Inc., Sunnyvale, CA.

(54) Patton, Charles , Ph.D. Thesis, Michigan State University, E. Lansing, MI, 1982.

(55) Stallings, Merian S.; Schulman, Stephen G. Anal. Chim. Acta 1975 78, 483-486.

(56) Intel Corporation, Santa Clara, CA.

(57) MOS/LSI Data Book, Advanced Micro Devices, Inc., Sunnyvale, CA, 1980.

(58) Malmstadt, Howard V.; Enke, Christie G.; Crouch, Stanley R. "Electronics and Instrumentation for Scientists," Benjamin/Cummings, Menlo Park, CA, 1981.

(59) "Data Acquisition Component Handbook," Datel-Intersil, Mansfield, MA.

(60) "Data Acquisition Components and Subsystems," Analog Devices, Norwood, MA, 1980.

(61) "Linear Databook," National Semiconductor Corporation, Santa Clara, CA, 1978.

(62) "Silicon Photocells, PIN Silicon Photodiodes, GaAsP Photodiodes," Hamamatsu Corporation, Middlesex, NJ, 1980.

(63) Brodie, Leo , Starting FORTH, Prentice-Hall, New York, 1981.

(64) Hoffman, Phillip, Michigan State University, E. Lansing, MI, 1982.

(65) Siegmund, Walter P., "Fiber Optics," in "Handbook of Optics," Walter V. Driscoll, Ed., McGraw-Hill, New York, 1978, 13-1 to 13-26.

(66) "Light-Conducting Fibres," Information Fibre Optics No. 7008/1e, JENA GLASWERK SHOTT GEN., Mainz, West Germany.

(67) Dr. Gale Harris, Associate Professor, Department of Radiology and Department of Physics-Astronomy, personal communication, 1979, Michigan State University, E. Lansing, MI.

(68) Math, Irwin, "Simple fiber measurements," Laser Focus 1979 September, 75.

(69) Soini, Erkki; Hemmila, Illka Clin. Chem. 1979 25, 353-361.

(70) Scharpe, Simon L.; Cooremann, W. M.; Blomme, W. J.; Lackeman, G. M. Clin. Chem. 1976 22, 733-738.

(71) Wisdom, G. Brian Clin. Chem. 1976 22, 1243-1255.

(72) Froehlich, Peter Appl. Spec. Rev. 1976 12, 83-129.

(73) Rubin, Martin Adv. Clin. Chem. 1970 13, 163-269.